

# Left-left-right-right magnetic order in spin-1/2 Kitaev-Heisenberg chain

Wang Yang,<sup>1</sup> Chao Xu,<sup>2,3</sup> Alberto Nocera,<sup>4</sup> and Ian Affleck<sup>4</sup>

<sup>1</sup>*School of Physics, Nankai University, Tianjin 300071, China*

<sup>2</sup>*Kavli Institute for Theoretical Sciences, University of Chinese Academy of Sciences, Beijing 100190, China*

<sup>3</sup>*Institute for Advanced Study, Tsinghua University, Beijing 100084, China*

<sup>4</sup>*Department of Physics and Astronomy and Stewart Blusson Quantum Matter Institute, University of British Columbia, Vancouver, B.C., Canada, V6T 1Z1*

In this work, we perform a combination of analytical and numerical studies on the phase diagram of the spin-1/2 Kitaev-Heisenberg chain in the region of negative Kitaev and positive Heisenberg couplings. Apart from the antiferromagnetic phase, we find a magnetically ordered phase with left-left-right-right order and a gapless phase with central charge value  $c = 1$ , resolving the existing contradictory results in literature regarding this parameter region. In particular, the origin of the left-left-right-right phase is clarified based on a perturbative Luttinger liquid analysis. Using a coupled-chain method, we further show that the one-dimensional (1D) left-left-right-right order is able to give a quasi-1D explanation for the 2D stripy order of the same model on the honeycomb lattice.

## I. INTRODUCTION

One-dimensional (1D) generalized Kitaev spin models can be constructed from their two-dimensional (2D) counterparts<sup>1–7</sup> by selecting one row out of the honeycomb lattice, where the word “generalized” is used to emphasize the fact that additional interactions beyond the Kitaev interaction are also included in the model in order to describe real Kitaev materials<sup>8–11</sup>. Recently, motivated by the potential of the 1D studies in providing hints for the 2D Kitaev physics, there have been surging research efforts in studying 1D generalized Kitaev models<sup>12–33</sup>. On the other hand, in addition to being helpful for understanding 2D physics, 1D generalized Kitaev models contain intriguing strongly correlated physics on their own, and it has been established that these 1D models have complicated nonsymmorphic symmetry group structures<sup>26,30</sup>, leading to exotic properties including emergent  $SU(2)_1$  conformal invariance<sup>19,29,30</sup>, nonsymmorphic bosonization<sup>27,28</sup>, nonlocal string order parameters<sup>16,23</sup>, and magnetic phases breaking nonsymmorphic symmetries<sup>20</sup>.

The Kitaev-Heisenberg model<sup>3,4</sup> is an intensively studied prototypical type of generalized Kitaev models. The phase diagram of the 1D spin-1/2 Kitaev-Heisenberg model has been investigated in various works<sup>12,14,16,20</sup>. However, there are contradictory statements on the physics of this model in the vicinity of the ferromagnetic (FM) Kitaev point. There is a special point in the FM Kitaev region located at  $K = -2J < 0$ , which has a hidden  $SU(2)$  symmetry<sup>34,35</sup>. The problem concerns with the phase diagram between the  $K = -2J < 0$  point and the FM Kitaev point: While Ref. 12 claims that the region is a  $c = 1$  Luttinger liquid phase where  $c$  represents the central charge, it was found in Ref. 14,20 that the system is magnetically ordered. In addition to the discrepancies in the literature on the nature of the phase diagram of the model, there is no theoretical understanding on the origin of either the Luttinger liquid or the magnetic order in the region.

Motivated by the above questions, in this work, we perform a combination of analytical and numerical studies in the region  $\phi \in (\arctan 2, \pi/2)$ , in which  $K = -\sin(\phi)$  and  $J = \cos(\phi)$  are the Kitaev and Heisenberg interactions, respectively. Notice that the hidden  $SU(2)$  symmetric FM point is located at  $\phi = \arctan(2)$ . By a combination of perturbative Luttinger liquid analysis and density matrix renormalization group (DMRG) numerical simulations, we find that there is a magnetically ordered phase close to the  $K = -2J$  point shown by “LLRR” in the phase diagram in Fig. 1 (a), where the spin ordering exhibits a collinear left-left-right-right (LLRR) pattern, which is consistent with the finding in Ref. 14 (named as staggered- $xy$  order there) and different from the spiral phase identified in Ref. 20. The key spirit of the strategy is straightforward to understand. After a unitary transformation called four-sublattice rotation, the Hamiltonian can be decomposed into two parts, one part the easy-plane XXZ model, and the other part a four-site periodic term. Since the Luttinger parameter diverges when the system approaches the  $K = -2J$  point, the system is very sensitive to perturbations, and as a result, driven into an ordered state by the four-site periodic term. The predictions are supported by our DMRG<sup>36–38</sup> simulations.

Furthermore, our DMRG numerics indicate that there exists a phase transition point  $\phi_{c1}$  which separates the LLRR phase from a  $c = 1$  gapless phase. Therefore, unlike the claims in the literatures<sup>12,14,20</sup>, the system have both ordered and gapless phases in the region  $\phi \in (\arctan(2), \pi/2)$ . Since the  $c = 1$  phase is close to the FM Kitaev point which has exponentially large ground state degeneracy, the numerics in the gapless phase are very difficult. An analytical understanding of the gapless phase remains unclear and will be left for future investigations.

We make two extensions of the LLRR phase in the 1D spin-1/2 Kitaev-Heisenberg model. First, by weakly coupling an infinite number of chains on the honeycomb lattice, we recover the stripy phase in the 2D

Kitaev-Heisenberg<sup>5,34</sup>, thereby providing a quasi-1D understanding to the 2D stripy phase. Second, by adding a Gamma term, we find that the LLRR phase extends to a finite region in the phase diagram of the spin-1/2 Kitaev-Heisenberg-Gamma chain shown in Fig. 1 (b).

The rest of the paper is organized as follows. In Sec. II, the model Hamiltonian is introduced and the symmetry group is analyzed. In Sec. III, the magnetic order in the 1D spin-1/2 Kitaev-Heisenberg model is determined by a combination of perturbative Luttinger liquid analysis and DMRG numerics. Sec. IV generalizes the analysis to the Kitaev-Heisenberg-Gamma chain. In Sec. V, the FM phase in the FM Heisenberg region is discussed based on a Luttinger liquid analysis. Sec. VI provides DMRG numerical evidence to the analytical results in the preceding sections. Sec. VII is devoted to a derivation of the stripy phase in the 2D Kitaev-Heisenberg model using a coupled chain method. Sec. VIII summarizes the main results of the paper.

## II. MODEL HAMILTONIAN AND SYMMETRIES

### A. Model Hamiltonian

We consider the 1D spin-1/2 Kitaev-Heisenberg model defined by the following Hamiltonian,

$$H_0 = \sum_{\langle ij \rangle \in \gamma \text{ bond}} [K S_i^\gamma S_j^\gamma + J \vec{S}_i \cdot \vec{S}_j], \quad (1)$$

in which  $i, j$  are two sites of nearest neighbors;  $\gamma = x, y$  is the spin direction associated with the  $\gamma$  bond connecting sites  $i$  and  $j$ , with the pattern shown in Fig. 2 (a);  $K$  and  $J$  are the Kitaev and Heisenberg couplings, respectively. A useful parametrization is

$$\begin{aligned} J &= \cos(\phi), \\ K &= -\sin(\phi). \end{aligned} \quad (2)$$

in which  $\phi \in [0, 2\pi]$ .

There is a self-duality transformation  $U_4$  of the Kitaev-Heisenberg model called four-sublattice rotation defined by<sup>34,35</sup>

$$\begin{aligned} \text{Sublattice 1 : } & (x, y, z) \rightarrow (-x', y', -z'), \\ \text{Sublattice 2 : } & (x, y, z) \rightarrow (-x', -y', z'), \\ \text{Sublattice 3 : } & (x, y, z) \rightarrow (x', -y', -z'), \\ \text{Sublattice 4 : } & (x, y, z) \rightarrow (x', y', z'), \end{aligned} \quad (3)$$

in which ‘‘Sublattice  $i$ ’’ ( $1 \leq i \leq 4$ ) represents all the sites  $i + 4n$  ( $n \in \mathbb{Z}$ ) in the chain, and the spin operators  $S^\alpha$  ( $\alpha = x, y, z$ ) are abbreviated as  $\alpha$  for simplicity. It can be verified that the Hamiltonian  $H'_0 = U_4 H_0 U_4^{-1}$  in the four-sublattice rotated frame is of the same form as Eq. (1) except that  $K$  and  $J$  should be replaced by  $K +$

$2J, -J$ , respectively. Hence  $U_4$  establishes the following equivalence relation in the parameter space,

$$(K, J) \simeq (K + 2J, -J). \quad (4)$$

Particularly,  $U_4$  reveals two hidden SU(2) symmetric points  $K = -2J < 0$  and  $K = -2J > 0$ , corresponding to FM and antiferromagnetic (AFM) Heisenberg model, respectively. From here on, we will call the frames before and after the  $U_4$  transformation as the original and  $U_4$  frames, respectively.

Although we mostly focus on the Kitaev-Heisenberg model in this work, the spin-1/2 Kitaev-Heisenberg-Gamma model will also be briefly discussed by introducing an additional Gamma term into Eq. (1). The Hamiltonian  $H_1$  of the Kitaev-Heisenberg-Gamma model is given by

$$H_1 = \sum_{\langle ij \rangle \in \gamma \text{ bond}} [K S_i^\gamma S_j^\gamma + J \vec{S}_i \cdot \vec{S}_j + \Gamma(S_i^\alpha S_j^\beta + S_i^\beta S_j^\alpha)], \quad (5)$$

in which the pattern of the  $\gamma$  bond is shown in Fig. 2 (a); and  $\alpha \neq \beta$  are the two remaining spin directions other than  $\gamma$ . Since  $\Gamma$  changes sign under a global spin rotation around  $z$ -axis by  $\pi$  whereas  $K$  and  $J$  remain unchanged, we have the equivalence

$$(K, J, \Gamma) \simeq (K, J, -\Gamma). \quad (6)$$

As a result of Eq. (6), it is enough to consider the  $\Gamma > 0$  region. After the  $U_4$  transformation, the Hamiltonian  $H'_1 = U_4 H_1 U_4^{-1}$  becomes

$$\begin{aligned} H'_1 &= \sum_{\langle ij \rangle \in \gamma \text{ bond}} [(K + 2J) S_i'^\gamma S_j'^\gamma - J \vec{S}_i' \cdot \vec{S}_j' \\ &\quad + \epsilon(\gamma) \Gamma(S_i'^\alpha S_j'^\beta + S_i'^\beta S_j'^\alpha)], \end{aligned} \quad (7)$$

in which the bonds  $\gamma = x, y, \bar{x}, \bar{y}$  has a four-site periodicity as shown in Fig. 2 (b); the function  $\epsilon(\gamma)$  is defined as  $\epsilon(x) = \epsilon(y) = -\epsilon(\bar{x}) = -\epsilon(\bar{y}) = 1$ ; and  $S_i'^\lambda = S_i'^\lambda$  ( $\lambda = x, y, z$ ). Notice that in this case,  $H'_1$  does not have the same form as  $H_1$ .

### B. Symmetries

We give a brief review of the symmetry group structures of  $H_0$  and  $H_1$ , which have been discussed in Ref. 20. In addition, we supplement the analysis in Ref. 20 with the short exact sequences satisfied by the symmetry groups, which provide rigorous discussions for the non-symmmorphic structures of the groups.

The Kitaev-Heisenberg model in Eq. (1) in the original frame is invariant under the following symmetry trans-

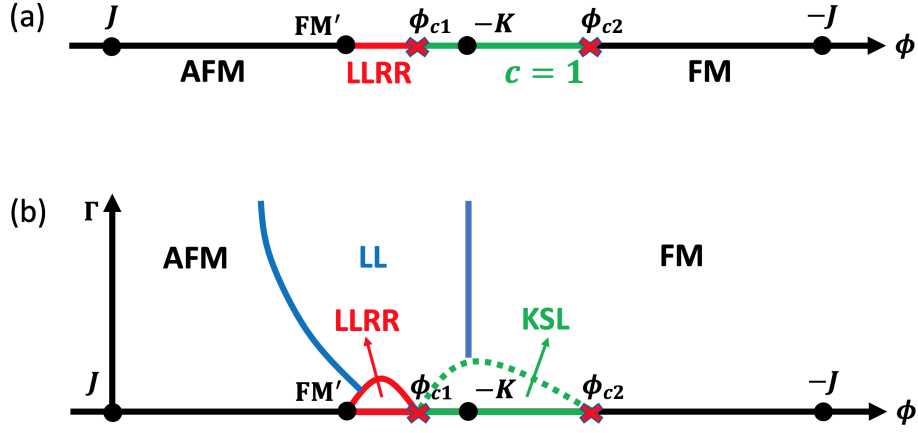


FIG. 1: Schematic plot of the phase diagrams of the 1D spin-1/2 (a) Kitaev-Heisenberg model and (b) Kitaev-Heisenberg-Gamma model in the parameter region  $\phi \in (0, \pi)$ . In both (a,b), in terms of the parametrization in Eq. (2), the  $J$ ,  $\text{FM}'$ ,  $-K$ ,  $J$  points on the horizontal axis have  $\phi$ -values  $0$ ,  $\arctan(2)$ ,  $\pi/2$ ,  $\pi$ , respectively, where  $\text{FM}'$  is the hidden  $\text{SU}(2)$  symmetric point satisfying  $K = -2J < 0$ . In (b), the vertical axis is  $\Gamma$ , and because of the equivalence in Eq. (6), only the  $\Gamma > 0$  region is shown.

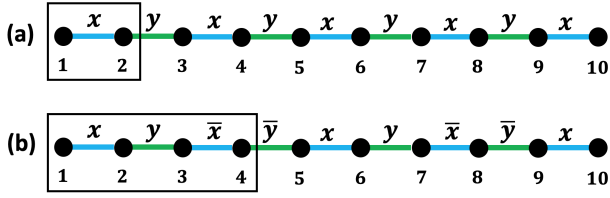


FIG. 2: Bond pattern of the Kitaev-Heisenberg-Gamma model (a) in the original frame and (b) in the four-sublattice rotated frame.

formations,

$$\begin{aligned}
 T &: (S_i^x, S_i^y, S_i^z) \rightarrow (-S_i^x, -S_i^y, -S_i^z) \\
 T_{2a} &: (S_i^x, S_i^y, S_i^z) \rightarrow (S_{i+2}^x, S_{i+2}^y, S_{i+2}^z) \\
 T_a I &: (S_i^x, S_i^y, S_i^z) \rightarrow (S_{-i+1}^x, S_{-i+1}^y, S_{-i+1}^z) \\
 R(\hat{y}, \pi) &: (S_i^x, S_i^y, S_i^z) \rightarrow (-S_i^x, S_i^y, -S_i^z) \\
 R(\hat{z}, -\frac{\pi}{2}) T_a &: (S_i^x, S_i^y, S_i^z) \rightarrow (-S_{i+1}^y, S_{i+1}^x, S_{i+1}^z), \quad (8)
 \end{aligned}$$

in which  $T$  is time reversal;  $T_{na}$  ( $n \in \mathbb{Z}$ ) is translation by  $n$  lattice sites;  $I$  is the spatial inversion with the inversion center located at site 0; and  $R(\hat{n}, \theta)$  denotes the global spin rotation around the  $\hat{n}$ -direction by an angle  $\theta$ . The symmetry group  $G_0$  of the Kitaev-Heisenberg chain is

$$G_0 = \langle T, T_{2a}, T_a I, R(\hat{y}, \pi), R(\hat{z}, -\frac{\pi}{2}) T_a \rangle, \quad (9)$$

where  $\langle \dots \rangle$  denotes the group generated by the elements within the bracket.

Since  $T_{4a} = [R(\hat{z}, -\frac{\pi}{2}) T_a]^4$  is a symmetry element and the abelian group  $\langle T_{4a} \rangle$  is a normal subgroup of  $G_0$ , it is legitimate to consider the quotient group  $G_0 / \langle T_{4a} \rangle$ .<sup>40</sup> It has been proved in Ref. 20 that  $G_0 / \langle T_{4a} \rangle$  is isomorphic to

$(\mathbb{Z}_2 \times \mathbb{Z}_2) \times D_{4h}$ , in which  $\mathbb{Z}_2 \times \mathbb{Z}_2 = \langle T_a I, T_{2a} \rangle / \langle T_{4a} \rangle$  and  $D_{4h} = \langle T \rangle \times D_4$ , where  $D_4$  is the dihedral group of order 8 given by  $D_4 = \langle R(\hat{z}, -\frac{\pi}{2}) T_a, R(\hat{y}, \pi) T_a I \rangle / \langle T_{4a} \rangle$ . We note that an intuitive way to understand the origin of the  $D_4$  group is by observing that if the spatial operations  $T_a$  and  $T_a I$  are removed from  $R(\hat{z}, -\frac{\pi}{2}) T_a$  and  $R(\hat{y}, \pi) T_a I$ , then the actions in the spin space  $\langle R(\hat{z}, -\frac{\pi}{2}), R(\hat{y}, \pi) \rangle$  generate the symmetry group of a spin square shown in Fig. 3, which is exactly the  $D_4$  group. As a consequence of the above analysis of the group structure of  $G_0$ , we have the short exact sequence

$$1 \rightarrow \langle T_{4a} \rangle \rightarrow G_0 \rightarrow (\mathbb{Z}_2 \times \mathbb{Z}_2) \times D_{4h} \rightarrow 1. \quad (10)$$

The group  $G_0$  is nonsymmorphic in the sense that the above short exact sequence is non-splitting, i.e., there is no way to embed the quotient group  $G_0 / \langle T_{4a} \rangle$  into  $G_0$ .

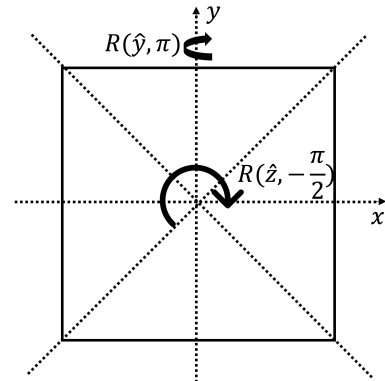


FIG. 3:  $R(\hat{y}, \pi)$  and  $R(\hat{z}, -\pi/2)$  as symmetry operations of a square in the spin space, in which the  $z$ -direction is perpendicular to the plane. The figure is taken from Ref. 20.

In Ref. 20, it is further shown that the symmetry group

$G_1$  of the Kitaev-Heisenberg-Gamma model in Eq. (5) in the original frame is

$$G_1 = \langle T, T_a I, R(\hat{n}_1, \pi) T_a \rangle, \quad (11)$$

in which  $\hat{n}_1 = \frac{1}{\sqrt{2}}(1, -1, 0)^T$  and  $R(\hat{n}_1, \pi) T_a = R(\hat{y}, \pi) R(\hat{z}, -\frac{\pi}{2}) T_a$ . The group  $G_1$  satisfies  $G_1 / \langle T_{4a} \rangle = \mathbb{Z}_2 \times C_{4h}$ , in which  $\mathbb{Z}_2 = \langle T_a I \rangle$  and  $C_{4h} = \langle T \rangle \times C_4$  where  $C_4 = \langle R(\hat{n}_1, \pi) T_a \rangle / \langle T_{4a} \rangle$  is the cyclic group of order 4. Therefore, there is the short exact sequence

$$1 \rightarrow \langle T_{4a} \rangle \rightarrow G_1 \rightarrow \mathbb{Z}_2 \times C_{4h} \rightarrow 1, \quad (12)$$

and  $G_1$  is again a nonsymmorphic group since the above short exact sequence is non-splitting. Clearly, the quotient  $\mathbb{Z}_2 \times C_{4h}$  in Eq. (12) is a subgroup of  $(\mathbb{Z}_2 \times \mathbb{Z}_2) \times D_{4h}$  in Eq. (10), as  $G_1$  is a subgroup of  $G_0$ .

On the other hand, the symmetry group  $G'_1$  of the Kitaev-Heisenberg-Gamma model in the  $U_4$  frame in Eq. (7) is given by

$$G'_1 = \langle T, R(\hat{y}, \pi) T_a I, R(\hat{z}, -\frac{\pi}{2}) T_a \rangle, \quad (13)$$

which is a nonsymmorphic group and satisfies

$$1 \rightarrow \langle T_{4a} \rangle \rightarrow G'_1 \rightarrow D_{4h} \rightarrow 1. \quad (14)$$

We note that  $G_1$  and  $G'_1$  is isomorphic to each other since they are the symmetry groups of the same model albeit in different frames. This is indeed true, as can be seen from the isomorphism  $\mathbb{Z}_2 \times C_{4h} \cong D_{4h}$ .

For all above nonsymmorphic symmetry groups, the non-splitting property can be most easily seen by considering the subgroup  $\langle R(\hat{z}, -\frac{\pi}{2}) T_a \rangle$  and the following short exact sequence,

$$1 \rightarrow \langle T_{4a} \rangle \rightarrow \langle R(\hat{z}, -\frac{\pi}{2}) T_a \rangle \rightarrow C_4 \rightarrow 1, \quad (15)$$

in which  $C_4 \cong \langle R(\hat{z}, -\frac{\pi}{2}) T_a \rangle / \langle T_{4a} \rangle$ . Replacing the groups in Eq. (15) with their isomorphic counterparts, Eq. (15) can be alternatively written as

$$1 \rightarrow 4\mathbb{Z} \rightarrow \mathbb{Z} \rightarrow \mathbb{Z}_4 \rightarrow 1, \quad (16)$$

which is clearly non-splitting (namely,  $\mathbb{Z}_4$  cannot be viewed as a subgroup of  $\mathbb{Z}$  in the sense of embedding), where  $\mathbb{Z}_4 = \mathbb{Z}/4\mathbb{Z}$ .

### C. Phase diagram

Before going to technical discussions, we give a description of the phase diagram shown in Fig. 1. We first consider the phase diagram of the Kitaev-Heisenberg model shown in Fig. 1 (a). The AFM Heisenberg point  $J$ , FM Heisenberg point  $-J$ , and the FM Kitaev point  $-K$  are located at  $\phi = 0$ ,  $\phi = \pi$ , and  $\phi = \pi/2$ , respectively. There is another special point  $FM'$  at  $\phi = \arctan(2)$ , which is a hidden  $SU(2)$  symmetric point satisfying  $K =$

$-2J < 0$ . We note that the region  $\phi \in (\arctan(2), \pi/2)$  is related to  $\phi \in (\pi/2, \pi)$  by the  $U_4$  transformation, hence the physics in these two regions are unitarily equivalent.

The phase diagram in Fig. 1 (a) divides into five phases: AFM phase between  $J$  and  $FM'$ ; LLRR phase between  $FM'$  and  $\phi_{c1} \approx 0.4\pi$ ; a gapless  $c = 1$  phase between  $\phi_{c1}$  and  $-K$ , where  $c$  represents the central charge; another  $c = 1$  phase between  $-K$  and  $\phi_{c2} \approx 0.56\pi$ , which is dual to the  $c = 1$  phase to the left of the  $-K$  point in Fig. 1 (a) under the  $U_4$  transformation; and an FM phase between  $\phi_{c2}$  and  $-J$ , which is dual to the LLRR phase in the region  $\phi \in [FM', \phi_{c1}]$  under the  $U_4$  transformation. The spin ordering has a four-site periodicity in the LLRR phase, aligning along  $\hat{x}, \hat{x}, -\hat{x}, -\hat{x}$  or  $\hat{y}, \hat{y}, -\hat{y}, -\hat{y}$  directions in a four-site unit cell, hence the name LLRR (left-left-right-right for short). We note that the LLRR phase was erroneously identified as a spiral phase in Ref. 20. The numerics become very difficult in the  $c = 1$  phase, since the system is very close to the FM Kitaev point, which is exactly solvable and has an exponentially large infinite ground state degeneracy in the thermodynamic limit (degeneracy is  $2^{L/2}$  for a system of  $L$  sites). Whether the low energy theory of the  $c = 1$  phase is a Luttinger liquid with an emergent  $U(1)$  symmetry or two Majorana fermions without emergent  $U(1)$  symmetry remains unclear, which will be left for future investigations.

By adding a small Gamma interaction, nearly all the phases extend to a finite area in the two-parameter phase diagram as shown in Fig. 1 (b). In particular, the LLRR phase on the  $\Gamma = 0$  line extends to the d-LLRR phase, where ‘‘d-LLRR’’ is ‘‘distorted-left-left-right-right’’ for short, the name of which comes from the fact that the spins are no longer collinear in this case. Whether the gapless  $c = 1$  phase on the horizontal axis extends to a finite region remains unclear, which is denoted as ‘‘KSL’’ (‘‘Kitaev spin liquid’’ for short) in Fig. 1 (b) and will be left for future studies. When  $\Gamma$  becomes larger, there appears a Luttinger liquid phase in the positive  $J$  region denoted as ‘‘LL’’ in Fig. 1, which has been discussed in detail in Ref. 20.

### III. PERTURBATIVE LUTTINGER LIQUID ANALYSIS OF THE KITAEV-HEISENBERG MODEL

In this section, we provide an analytical understanding for the origin of the LLRR phase in the spin-1/2 Kitaev-Heisenberg chain based on a perturbative Luttinger liquid analysis. We will work in the  $U_4$  frame unless otherwise stated. Since the region between  $-K$  and  $-J$  is dual to the region between  $FM'$  and  $-K$ , the perturbative Luttinger liquid analysis can also be applied to explain the FM phase for  $\phi \in [\phi_{c2}, \pi]$ .

### A. Failure of the classical analysis

The simplest approach is the classical analysis by treating the spin operators as vectors of real numbers which is valid in the large- $S$  limit. We will show that the classical analysis leads to an infinitely degenerate ground state manifold, and fails since it ignores the quantum fluctuations.

In the classical analysis, the spin operator  $\vec{S}_i$  is approximated as

$$\vec{S}_i = S(x_i, y_i, z_i)^T, \quad (17)$$

in which  $S$  is the value of the spin, and  $x_i, y_i, z_i$  are normalized as

$$(x_i)^2 + (y_i)^2 + (z_i)^2 = 1. \quad (18)$$

Assuming that the ground state has a two-site periodicity, i.e.,  $\vec{S}_{i+2} = \vec{S}_i$ , the classical free energy per two-site unit cell in the  $U_4$  frame becomes

$$f = (K + 2J)S^2(x'_1 x'_2 + y'_1 y'_2) - 2JS^2 \hat{n}'_1 \cdot \hat{n}'_2 - \frac{1}{2}\lambda_1(\hat{n}'_1 \cdot \hat{n}'_1 - 1) - \frac{1}{2}\lambda_2(\hat{n}'_2 \cdot \hat{n}'_2 - 1), \quad (19)$$

in which  $\hat{n}'_i = (x'_i, y'_i, z'_i)$ , and  $\lambda_i$  ( $i = 1, 2$ ) are introduced as a Lagrange multiplier to impose the constraints in Eq. (18). Eq. (19) can be rewritten as

$$f = (-2J + \delta)S^2(x'_1 x'_2 + y'_1 y'_2) - 2JS^2 z'_1 z'_2 - \frac{1}{2}\lambda_1(\hat{n}'_1 \cdot \hat{n}'_1 - 1) - \frac{1}{2}\lambda_2(\hat{n}'_2 \cdot \hat{n}'_2 - 1), \quad (20)$$

in which  $\delta = K + 2J$ . In the region between FM' and  $-K$  in Fig. 1 (a), we have  $J > 0$  and  $\delta < 0$ . Therefore, an FM configuration within the  $xy$ -plane is able to lower the energy in Eq. (20). However, it is clear that the free energy  $f$  in Eq. (20) has a U(1) symmetry, corresponding to a rotational symmetry around the  $z$ -axis. Hence, the classical ground states are infinitely degenerate, since the FM spin direction can point to any direction within the  $xy$ -plane. This is clearly absurd, since the system only has discrete symmetries and cannot develop a symmetry breaking pattern which has a continuously variable spin orientation.

Quantum fluctuations will break the infinite classical ground state degeneracy. There are two possibilities though. The system either becomes a gapless Luttinger liquid (like the easy-plane XXZ model where the classical analysis also gives an infinite ground state degeneracy but the system is gapless at the quantum level), or is magnetically ordered but with a discrete spontaneous symmetry breaking pattern. We will show that at quantum level, the Luttinger liquid behavior is unstable under the symmetry allowed perturbations, and as a result, the system develops a magnetic order with a discrete symmetry breaking pattern.

### B. Perturbative Luttinger liquid analysis

In the  $U_4$  frame, we write the Hamiltonian in the region  $\phi \in (\arctan 2, \pi/2)$  as

$$H'_0 = H'_{XXZ} + \frac{1}{2}\delta \sum_i (-)^{i-1} (S'_i S'_{i+1}{}^x - S'_i{}^y S'_{i+1}{}^y), \quad (21)$$

in which

$$H'_{XXZ} = \sum_i [(-J + \frac{1}{2}\delta)(S'_i S'_{i+1}{}^x + S'_i{}^y S'_{i+1}{}^y) - JS'_i{}^z S'_{i+1}{}^z], \quad (22)$$

and

$$\delta = K + 2J < 0. \quad (23)$$

It can be seen that  $H'_{XXZ}$  represents an easy-plane XXZ model when  $\delta < 0$ , hence lies in the gapless Luttinger liquid phase. The strategy is to take the second term in Eq. (21) as a perturbation and analyze its effects using the Luttinger liquid theory. We emphasize that the problem is non-perturbative in nature, since the coupling constant  $\frac{1}{2}\delta$  in the second term of  $H'_0$  is comparable with the difference between the transverse and longitudinal couplings in  $H'_{XXZ}$  in Eq. (22). Therefore, the perturbative Luttinger liquid analysis to be discussed below is not analytically controllable in the most rigorous sense, and must be verified by numerical simulations.

For later convenience, we further consider a two-sublattice rotation  $V_2$  defined as

$$\begin{aligned} \text{Sublattice 1 : } & (x', y', z') \rightarrow (x'', y'', z''), \\ \text{Sublattice 2 : } & (x', y', z') \rightarrow (-x'', -y'', z''), \end{aligned} \quad (24)$$

in which ‘‘Sublattice  $i$ ’’ ( $1 \leq i \leq 2$ ) represents all the sites  $i + 2n$  ( $n \in \mathbb{Z}$ ) in the chain, and the spin symbol  $S$  in  $S^\alpha$  is dropped for simplicity. Then we obtain

$$H''_0 = H''_{XXZ} + H_\delta, \quad (25)$$

in which

$$\begin{aligned} H''_{XXZ} &= (J - \frac{1}{2}\delta) \sum_i [S''_i{}^x S''_{i+1}{}^x + S''_i{}^y S''_{i+1}{}^y + \Delta S''_i{}^z S''_{i+1}{}^z], \\ H_\delta &= \frac{1}{2}\delta \sum_i (-)^i (S''_i{}^x S''_{i+1}{}^x - S''_i{}^y S''_{i+1}{}^y), \end{aligned} \quad (26)$$

where

$$\Delta = -\frac{J}{J - \frac{1}{2}\delta}. \quad (27)$$

The advantage of  $V_2$  is that the correlation functions of  $H''_{XXZ}$  in the  $xy$ -plane are rendered to be dominated by AFM rather than FM fluctuations, which is the commonly used convention in Luttinger liquid theory. After

applying the  $V_2$  transformation, the symmetry operations in Eq. (8) become

$$\begin{aligned} V_2 T (V_2)^{-1} &= T \\ V_2 T_{2a} (V_2)^{-1} &= T_{2a} \\ V_2 T_a I (V_2)^{-1} &= R(\hat{z}'', \pi) T_a I \\ V_2 R(\hat{y}'', \pi) (V_2)^{-1} &= R(\hat{y}'', \pi) \\ V_2 R(\hat{z}'', -\frac{\pi}{2}) T_a (V_2)^{-1} &= R(\hat{z}'', \frac{\pi}{2}) T_a. \end{aligned} \quad (28)$$

The easy-plane XXZ model  $H''_{XXZ}$  for  $\delta < 0$  can be bosonized in the standard way. The low energy physics of  $H''_{XXZ}$  is described by the following Luttinger liquid theory,

$$H_{LL} = \frac{v}{2} \int dx \left[ \frac{1}{\kappa} (\nabla\varphi)^2 + \kappa (\nabla\theta)^2 \right], \quad (29)$$

in which  $v$  is the velocity,  $\kappa$  is the Luttinger liquid parameter, and the  $\theta$  and  $\varphi$  fields satisfy the commutation relation  $[\varphi(x), \theta(x')] = \frac{i}{2} \text{sgn}(x' - x)$ . The local spin operators of the XXZ model is related to the boson fields  $\theta, \varphi$  via the following bosonization formulas

$$\begin{aligned} S''z(x) &= -\frac{1}{\sqrt{\pi}} \nabla\varphi(x) + \text{const.} \frac{1}{a} (-)^n \cos(2\sqrt{\pi}\varphi(x)), \\ S''+(x) &= \text{const.} \frac{1}{\sqrt{a}} e^{-i\sqrt{\pi}\theta(x)} [(-)^n + \cos(2\sqrt{\pi}\varphi(x))], \end{aligned} \quad (30)$$

in which  $S''+ = S''x + iS''y$ , and  $x = na$  ( $n \in \mathbb{Z}$ ) is the spatial coordinate in the continuum limit. The easiest way to treat the perturbation  $H_\delta$  is to do a first order perturbation, namely, rewriting  $H_{LL}$  in terms of the  $\theta, \varphi$  fields by replacing the spin operators in  $H_\delta$  with the expressions in Eq. (30). The first order projection can be evaluated as

$$\begin{aligned} \sum_i (-)^i (S''x_i S''x_{i+1} - S''y_i S''y_{i+1}) &= \\ \frac{(\text{const.})^2}{a^2} \int dx & \left[ \cos(\sqrt{\pi}\theta(x)) \cos(\sqrt{\pi}\theta(x+a)) \right. \\ & \left. - \sin(\sqrt{\pi}\theta(x)) \sin(\sqrt{\pi}\theta(x+a)) \right] \\ & \times [\cos(2\sqrt{\pi}\varphi(x+a)) - \cos(2\sqrt{\pi}\varphi(x))] + \dots, \end{aligned} \quad (31)$$

in which “ $\dots$ ” denotes the terms not included in the first order projection. Eq. (31) can be simplified using the operator product expansions of vertex operators. However, we don't need to bother ourselves to perform such simplifications, since the operators in Eq. (31) are highly irrelevant in the vicinity of the FM' point in the sense of renormalization group (RG). To see this, notice that the scaling dimension of  $\cos(2\sqrt{\pi}\varphi)$  is  $\kappa$ , where  $\kappa$  is the Luttinger parameter. However,  $\kappa$  diverges when the easy-plane XXZ model approaches the FM limit, i.e., when  $\Delta \rightarrow -1$  ( $|\Delta| < 1$ ) in Eq. (26). This is exactly the case when  $\delta$  in Eq. (26) is small. Hence we see that

when  $|\delta| \ll 1$ , Eq. (31) has a very large scaling dimension, therefore can be neglected in the Luttinger liquid theory when low energy physics is considered.

The above analysis shows that we need to go beyond first order projection. Since such calculations are difficult, we will not explicitly derive the high order perturbations. Instead, we use a symmetry analysis to figure out the most relevant symmetry allowed terms in the RG sense. It is worth to note that although the symmetry analysis is able to determine the form of the corresponding relevant operator, the signs and order of magnitudes of the coupling constants cannot be figured out. For our purpose, the order of magnitude of the coupling constant is not important, whereas the sign is crucial which determines the specific type of magnetic instability. We will infer the sign of the coupling constant indirectly by numerical calculations in later sections.

To perform the symmetry analysis, the transformation properties of the  $\theta, \varphi$  fields are needed. Such transformations can be derived by first performing a Jordan-Wigner transformation to the spin operators, then bosonizing the obtained spinless fermion. The results are (for details, see Appendix A)

$$\begin{aligned} T : \theta(t, x) &\rightarrow \theta(-t, x) + \sqrt{\pi}, \varphi(t, x) \rightarrow -\varphi(-t, x), \\ \eta_r^\dagger &\rightarrow \eta_{-r}, \\ T_a : \theta &\rightarrow \theta + \sqrt{\pi}, \varphi \rightarrow \varphi + \sqrt{\pi}/2, \eta_r^\dagger \rightarrow \eta_r^\dagger, \\ I : \theta(t, x) &\rightarrow \theta(t, -x), \varphi(t, x) \rightarrow -\varphi(t, -x) + \sqrt{\pi} S_T^z, \\ \eta_r^\dagger &\rightarrow \eta_{-r}^\dagger, \\ R(\hat{y}'', \pi) : \theta &\rightarrow -\theta + \sqrt{\pi}, \varphi \rightarrow -\varphi, \eta_r^\dagger \rightarrow \eta_r, \\ R(\hat{z}'', \beta) : \theta &\rightarrow \theta + \beta/\sqrt{\pi}, \varphi \rightarrow \varphi, \eta_r^\dagger \rightarrow \eta_r^\dagger, \end{aligned} \quad (32)$$

where  $\eta_r$  ( $r = L, R$ ) are the Klein factors for the left and right movers of the spinless fermion, and  $S_T^z = \sum_{k \in \mathbb{Z}} S_k^z$  is the total spin along  $z$ -direction, which is a good quantum number for the XXZ chain.

Next we analyze what vertex operators are allowed by symmetries. First notice that only operators of the form  $e^{i\sqrt{\pi}(2n\varphi+m\theta)}$  are allowed, since the bosonization formulas for the spin operators in Eq. (30) only contain  $\pm 2\sqrt{\pi}\varphi, \pm\sqrt{\pi}\theta$  in the exponentials, and a perturbation, whatever its order, can only give integer multiples of  $2\sqrt{\pi}\varphi$  and  $\sqrt{\pi}\theta$ . Since the scaling dimension of  $e^{2i\lambda\sqrt{\pi}\varphi}$  ( $\lambda \in \mathbb{Z}$ ) diverges when  $|\delta| \ll 1$ , we consider  $e^{im\sqrt{\pi}\theta}$ , which are the only possible relevant vertex operators at low energies.

Using Eq. (32), the transformations of  $\cos(m\sqrt{\pi}\theta)$  and  $\sin(m\sqrt{\pi}\theta)$  ( $m \in \mathbb{Z}$ ) under the symmetries operations in Eq. (8) can be derived as

$$\begin{aligned} T : \cos(m\sqrt{\pi}\theta) &\rightarrow (-)^m \cos(m\sqrt{\pi}\theta), \\ \sin(m\sqrt{\pi}\theta) &\rightarrow (-)^m \sin(m\sqrt{\pi}\theta), \end{aligned} \quad (33)$$

$$\begin{aligned} T_{2a} : \cos(m\sqrt{\pi}\theta) &\rightarrow \cos(m\sqrt{\pi}\theta), \\ \sin(m\sqrt{\pi}\theta) &\rightarrow \sin(m\sqrt{\pi}\theta), \end{aligned} \quad (34)$$

$$R(\hat{z}'', \pi)T_a I : \begin{aligned} \cos(m\sqrt{\pi}\theta(x)) &\rightarrow \cos(m\sqrt{\pi}\theta(-x)), \\ \sin(m\sqrt{\pi}\theta(x)) &\rightarrow \sin(m\sqrt{\pi}\theta(-x)), \end{aligned} \quad (35)$$

$$R(\hat{y}'', \pi) : \begin{aligned} \cos(m\sqrt{\pi}\theta) &\rightarrow (-)^m \cos(m\sqrt{\pi}\theta), \\ \sin(m\sqrt{\pi}\theta) &\rightarrow (-)^{m+1} \sin(m\sqrt{\pi}\theta), \end{aligned} \quad (36)$$

$$R(\hat{z}'', \frac{\pi}{2})T_a : \begin{aligned} \cos(m\sqrt{\pi}\theta) &\rightarrow (-)^m \cos(m\sqrt{\pi}\theta + \frac{m\pi}{2}), \\ \sin(m\sqrt{\pi}\theta) &\rightarrow (-)^m \sin(m\sqrt{\pi}\theta + \frac{m\pi}{2}). \end{aligned} \quad (37)$$

Combining Eq. (33) with Eq. (36), it can be seen that  $\sin(m\sqrt{\pi}\theta)$  is forbidden, and  $m$  has to be an even integer for  $\cos(m\sqrt{\pi}\theta)$ . Then Eq. (37) requires  $\cos(4n\sqrt{\pi}\theta)$ , which is invariant under all symmetry transformations. Taking the smallest possible number  $n = 1$  (which has the smallest scaling dimension), the most relevant symmetry allowed perturbation is given by

$$g \int dx \cos(4\sqrt{\pi}\theta), \quad (38)$$

in which  $g$  is the coupling constant. The operator in Eq. (38) has a scaling dimension  $4/\kappa$ , which is highly relevant when  $\kappa$  becomes large. In fact,  $\kappa$  can be arbitrarily large in the vicinity of the FM' point in Fig. (1).

### C. Magnetic ordering

Next, we figure out the magnetic order arising from the operator in Eq. (38). We need to distinguish between two cases, i.e.,  $g > 0$  and  $g < 0$ .

We first consider  $g > 0$ . In this case, the energy in Eq. (38) is minimized at  $4\sqrt{\pi}\theta = (2n+1)\pi$ , i.e.,

$$\theta_n^{(I)} = \frac{2n+1}{4}\sqrt{\pi}, \quad 0 \leq n \leq 3, \quad (39)$$

where the superscript “(I)” is used to denote the case  $g > 0$ . We take one of the four degenerate solutions at  $n = 0$  as an example, giving  $\theta_0^{(I)} = \frac{\sqrt{\pi}}{4}$ . Plugging  $\theta_0^{(I)}$  into the bosonization formulas in Eq. (30), the spin orientations can be determined as

$$\vec{S}_j^{(I)''} = (-)^j \frac{1}{\sqrt{2}}(1, 1, 0)^T. \quad (40)$$

Performing  $(V_2)^{-1}$  to Eq. (40), we obtain

$$\vec{S}_j^{(I)'} = \frac{1}{\sqrt{2}}(1, 1, 0)^T. \quad (41)$$

It is useful to determine the symmetry breaking pattern of Eq. (41). It can be verified that Eq. (41) is invariant under the following symmetry operations

$$H^{(I)} = \langle T_a I, T_{2a}, [R(\hat{z}, -\frac{\pi}{2})T_a]^2 T, R(\hat{z}, -\frac{\pi}{2})T_a \cdot R(\hat{y}, \pi)T_a I \rangle, \quad (42)$$

in which  $H^{(I)}$  is the unbroken symmetry group. Using a similar analysis as Ref. 20,  $H^{(I)}$  can be shown to satisfy

$$1 \rightarrow \langle T_{4a} \rangle \rightarrow H^{(I)} \rightarrow (\mathbb{Z}_2 \times \mathbb{Z}_2) \times D_2^{(I)} \rightarrow 1, \quad (43)$$

in which

$$\mathbb{Z}_2 \times \mathbb{Z}_2 = \langle T_a I, T_{2a} \rangle / \langle T_{4a} \rangle, \quad (44)$$

and

$$D_2^{(I)} = \langle [R(\hat{z}, -\frac{\pi}{2})T_a]^2 T, R(\hat{z}, -\frac{\pi}{2})T_a \cdot R(\hat{y}, \pi)T_a I \rangle / \langle T_{4a} \rangle, \quad (45)$$

where  $D_2^{(I)} \cong D_2$  is the dihedral group of order 4. Combining Eq. (10) with Eq. (42), we see that the symmetry breaking pattern is

$$(\mathbb{Z}_2 \times \mathbb{Z}_2) \times D_{4h} \rightarrow (\mathbb{Z}_2 \times \mathbb{Z}_2) \times D_2. \quad (46)$$

Since  $[(\mathbb{Z}_2 \times \mathbb{Z}_2) \times D_{4h}] / [(\mathbb{Z}_2 \times \mathbb{Z}_2) \times D_2] = 4$ , there are four degenerate configurations, consistent with the analysis in Eq. (39).

The most general magnetic pattern can be figured out by requiring invariance under  $H^{(I)}$ , which gives

$$\vec{S}_j^{(I)'} = N_1 \frac{1}{\sqrt{2}}(1, 1, 0)^T, \quad (47)$$

in which  $N_1$  is the magnitude of the spin ordering. Rotating back to the original frame by performing  $(U_4)^{-1}$ , we obtain

$$\begin{aligned} \vec{S}_{1+4n}^{(I)} &= N_1 \frac{1}{\sqrt{2}}(-1, 1, 0)^T, \\ \vec{S}_{2+4n}^{(I)} &= N_1 \frac{1}{\sqrt{2}}(-1, -1, 0)^T, \\ \vec{S}_{3+4n}^{(I)} &= N_1 \frac{1}{\sqrt{2}}(1, -1, 0)^T, \\ \vec{S}_{4+4n}^{(I)} &= N_1 \frac{1}{\sqrt{2}}(1, 1, 0)^T. \end{aligned} \quad (48)$$

This is a spiral phase in which the spins rotate in the  $xy$ -plane as the position is moved along the chain.

Next we consider the  $g < 0$  case. The energy in Eq. (38) is minimized at  $4\sqrt{\pi}\theta = 2n\pi$ , i.e.,

$$\theta_n^{(II)} = \frac{n}{2}\sqrt{\pi}, \quad 0 \leq n \leq 3, \quad (49)$$

We take one of the four degenerate solutions at  $n = 1$  as an example, giving  $\theta_0^{(II)} = \pi/2$ . Plugging  $\theta_0^{(II)}$  into the bosonization formulas in Eq. (30), the spin orientations can be determined as

$$\vec{S}_j^{(II)''} = (-)^j (0, 1, 0)^T. \quad (50)$$

Performing  $(V_2)^{-1}$  to Eq. (50), we obtain

$$\vec{S}_j^{(II)'} = \frac{1}{\sqrt{2}}(0, 1, 0)^T. \quad (51)$$

It can be verified that Eq. (51) is invariant under the following symmetry operations

$$H^{(\text{II})} = \langle T_a I, T_{2a}, [R(\hat{z}, -\frac{\pi}{2})T_a]^2 T, R(\hat{y}, \pi)T_a I \rangle, \quad (52)$$

in which  $H^{(\text{II})}$  is the unbroken symmetry group. Similarly,  $H^{(\text{II})}$  satisfies

$$1 \rightarrow \langle T_{4a} \rangle \rightarrow H^{(\text{II})} \rightarrow (\mathbb{Z}_2 \times \mathbb{Z}_2) \times D_2^{(\text{II})} \rightarrow 1, \quad (53)$$

in which

$$\mathbb{Z}_2 \times \mathbb{Z}_2 = \langle T_a I, T_{2a} \rangle / \langle T_{4a} \rangle, \quad (54)$$

and

$$D_2^{(\text{II})} = \langle [R(\hat{z}, -\frac{\pi}{2})T_a]^2 T, R(\hat{y}, \pi)T_a I \rangle / \langle T_{4a} \rangle, \quad (55)$$

where  $D_2^{(\text{II})} \cong D_2$ .

The general magnetic pattern can be figured out by requiring invariance under  $H^{(\text{II})}$ , which gives

$$\vec{S}_j^{(\text{II})'} = N_2(0, 1, 0)^T, \quad (56)$$

in which  $N_2$  is the magnitude of the spin ordering. Rotating back to the original frame by performing  $(U_4)^{-1}$ , we obtain

$$\begin{aligned} \vec{S}_{1+4n}^{(\text{II})} &= N_2(0, 1, 0)^T, \\ \vec{S}_{2+4n}^{(\text{II})} &= N_2(0, -1, 0)^T, \\ \vec{S}_{3+4n}^{(\text{II})} &= N_2(0, -1, 0)^T, \\ \vec{S}_{4+4n}^{(\text{II})} &= N_2(0, 1, 0)^T. \end{aligned} \quad (57)$$

This is a left-left-right-right magnetic order, in which the spins are along the  $y$ -direction and reverse their directions every two sites.

From the discussions in this section, we see that the sign of the coupling constant  $g$  is crucial to determine the magnetic pattern of the system. However, a pure symmetry analysis is not able to give the sign of  $g$ . The actual magnetic order developed in the system have to be determined by numerics as will be discussed in Sec. VI.

#### IV. LLRR PHASE IN THE KITAEV-HEISENBERG-GAMMA CHAIN

In this section, we apply the perturbative Luttinger liquid analysis to the Kitaev-Heisenberg-Gamma chain close to the FM' point, by adding a nonzero Gamma term. Because of the equivalence in Eq. (6), we will focus on the  $\Gamma > 0$  region.

The strategy is the same as Sec. IIIB, namely, figuring out the most relevant (in the RG sense) symmetry allowed term in the Luttinger liquid theory. The symmetry group  $G'_1$  of the Kitaev-Heisenberg-Gamma model in

the  $U_4$  frame given in Eq. (13) is used for this analysis. After applying the  $V_2$  transformation, the symmetry operations in Eq. (13) become  $T, R(\hat{x}'', \pi)T_a I, R(\hat{z}'', \frac{\pi}{2})T_a$ . The transformation properties of  $\sin(m\sqrt{\pi}\theta), \cos(m\sqrt{\pi}\theta)$  under  $T, R(\hat{z}'', \frac{\pi}{2})T_a$  have been given in Eq. (37), and for  $R(\hat{x}'', \pi)T_a I$ , the transformation rule is

$$\begin{aligned} R(\hat{x}'', \pi)T_a I : \cos(m\sqrt{\pi}\theta(x)) &\rightarrow (-)^m \cos(m\sqrt{\pi}\theta(-x)), \\ \sin(m\sqrt{\pi}\theta(x)) &\rightarrow (-)^{m+1} \sin(m\sqrt{\pi}\theta(-x)). \end{aligned} \quad (58)$$

This time,  $\sin(m\sqrt{\pi}\theta)$  is again forbidden, since it changes sign under  $TR(\hat{x}'', \pi)T_a I$ . Because of the symmetries  $T$  and  $R(\hat{z}'', -\frac{\pi}{2})T_a$ ,  $m$  has to be a multiple of 4 in  $\cos(m\sqrt{\pi}\theta)$ . Hence the low energy symmetry allowed term with the smallest scaling dimension is still given by Eq. (38).

Similar to the analysis in Sec. IIIC, we need to distinguish between the  $g > 0$  and  $g < 0$  cases. First consider the  $g > 0$  case. The energy is again minimized at values of  $\theta$  in Eq. (39). However, the unbroken symmetry group is different because of a reduction of the symmetry group of the model. It can be checked that the unbroken symmetry group  $H_1^{(1)}$  in the  $U_4$  frame (which is a subgroup of  $G'_1$  in Eq. (13) without the further  $V_2$  transformation) is given by

$$H_1^{(1)} = \langle [R(\hat{z}, -\frac{\pi}{2})T_a]^2 T, R(\hat{z}, -\frac{\pi}{2})T_a \cdot R(\hat{y}, \pi)T_a I \rangle, \quad (59)$$

which satisfies

$$1 \rightarrow \langle T_{4a} \rangle \rightarrow H_1^{(1)} \rightarrow D_2^{(1)} \rightarrow 1, \quad (60)$$

where  $D_2^{(1)}$  is still given by Eq. (45). The most general magnetic pattern with an unbroken symmetry group  $H_1^{(1)}$  in the  $U_4$  frame has been determined in Ref. 20 as

$$\begin{aligned} \vec{S}_1^{(1)} &= (f, f, 0)^T, \\ \vec{S}_2^{(1)} &= (k, k, h)^T, \\ \vec{S}_3^{(1)} &= (f, f, 0)^T, \\ \vec{S}_4^{(1)} &= (k, k, -h)^T. \end{aligned} \quad (61)$$

Rotating back to the original frame, the spin ordering is

$$\begin{aligned} \vec{S}_1^{(1)} &= (-f, f, 0)^T, \\ \vec{S}_2^{(1)} &= (-k, -k, h)^T, \\ \vec{S}_3^{(1)} &= (f, -f, 0)^T, \\ \vec{S}_4^{(1)} &= (k, k, -h)^T. \end{aligned} \quad (62)$$

This is a distorted spiral order, which gains components in the  $z$ -direction compared with the magnetic ordering in Eq. (48) for  $\Gamma = 0$ . Clearly, Eq. (48) can be obtained from Eq. (62) by setting  $f = k = \frac{1}{\sqrt{2}}N_1$  and  $h = 0$ .

Next consider the  $g < 0$  case. The energy is again minimized at values of  $\theta$  in Eq. (49). It can be checked that the unbroken symmetry group  $H_1^{(\text{II})}$  is given by

$$H_1^{(\text{II})} = \langle [R(\hat{z}, -\frac{\pi}{2})T_a]^2 T, R(\hat{y}, \pi)T_a I \rangle, \quad (63)$$

which satisfies

$$1 \rightarrow \langle T_{4a} \rangle \rightarrow H_1^{(\text{II})} \rightarrow D_2^{(\text{II})} \rightarrow 1, \quad (64)$$

where  $D_2^{(\text{II})}$  is still given by Eq. (45). The most general magnetic pattern with an unbroken symmetry group  $H_1^{(\text{II})}$  in the  $U_4$  frame can be determined as

$$\begin{aligned} \vec{S}_1^{(\text{II})} &= (0, b, -c)^T, \\ \vec{S}_2^{(\text{II})} &= (0, b, -c)^T, \\ \vec{S}_3^{(\text{II})} &= (0, b, c)^T, \\ \vec{S}_4^{(\text{II})} &= (0, b, c)^T. \end{aligned} \quad (65)$$

Rotating back to the original frame, the spin ordering is

$$\begin{aligned} \vec{S}_1^{(\text{II})} &= (0, b, c)^T, \\ \vec{S}_2^{(\text{II})} &= (0, -b, -c)^T, \\ \vec{S}_3^{(\text{II})} &= (0, -b, -c)^T, \\ \vec{S}_4^{(\text{II})} &= (0, b, c)^T. \end{aligned} \quad (66)$$

This is a distorted left-left-right-right magnetic order when  $a$  and  $b$  have the same signs having components along the  $z$ -direction as well. Clearly, Eq. (57) can be obtained from Eq. (66) by setting  $b = \frac{1}{\sqrt{2}}N_2$ ,  $c = 0$ .

Finally, we note that the  $c = 1$  phase in the Kitaev-Heisenberg model extends to a Kitaev spin liquid phase when  $\Gamma$  is nonzero as shown in Fig. 1 (c) (denoted as ‘‘KSL’’ in the figure), whose nature remains unclear and will be left for future investigations.

## V. THE FM PHASE IN THE $J < 0$ REGION

Although this work mainly focuses on the LLRR phase in the  $J > 0$  region, in this section we briefly discuss the FM phase in the  $J < 0$  region in Fig. 1 in the framework of perturbative Luttinger liquid analysis.

For the Kitaev-Heisenberg model, the region between  $-K$  and  $-J$  in Fig. 1 (a) is unitarily equivalent to the region between  $-K$  and FM' under the  $U_4$  transformation. Hence, in the neighborhood of  $-J$ , the system is in an ordered phase, and the magnetic pattern in the original frame in this case is exactly the same as the pattern in the  $U_4$  frame in the vicinity of FM'. Therefore, in the region  $[\phi_{c2}, \pi]$  in Fig. 1 (a) where  $\phi_{c2}$  is dual to  $\phi_{c1}$  under the equivalent relation in Eq. (4), we conclude that for  $g > 0$ , the magnetic ordering is along  $\frac{1}{\sqrt{2}}(\pm 1, \pm 1, 0)$ -directions (see Eq. (47) and the other three degenerate solutions); and for  $g < 0$ , the magnetic ordering is along

$\pm \hat{x}$ - and  $\pm \hat{y}$ -directions (see Eq. (56) and the other three degenerate solutions).

Next we consider the Kitaev-Heisenberg-Gamma model with a nonzero Gamma term. This time, the analysis in Sec. IIIB cannot be applied, since the perturbative Luttinger liquid analysis should now be applied in the original frame, not the four-sublattice rotated frame. Performing  $V_2$  in Eq. (24) to the Hamiltonian  $H_1$  in Eq. (67) in the original frame, the Hamiltonian  $\tilde{H}_1 = V_2 H_1 (V_2)^{-1}$  becomes

$$\tilde{H}_1 = \tilde{H}_{XXZ} + H_K + H_\Gamma, \quad (67)$$

in which

$$\tilde{H}_{XXZ} = |J + \frac{1}{2}K| \sum_i [\tilde{S}_i^x \tilde{S}_{i+1}^x + \tilde{S}_i^y \tilde{S}_{i+1}^y + \Delta \tilde{S}_i^z \tilde{S}_{i+1}^z], \quad (68)$$

$$H_K = \frac{1}{2}K \sum_i (-)^i (\tilde{S}_i^x \tilde{S}_{i+1}^x - \tilde{S}_i^y \tilde{S}_{i+1}^y), \quad (69)$$

$$H_\Gamma = \Gamma \sum_{\langle ij \rangle \in \gamma \text{ bond}} (\tilde{S}_i^\alpha \tilde{S}_j^\beta - \tilde{S}_i^\beta \tilde{S}_j^\alpha), \quad (70)$$

in which  $\tilde{S}_i$  represents the spin operators after the  $V_2$  transformation, and

$$\Delta = -\frac{J}{J + K/2}. \quad (71)$$

Notice that both  $J$  and  $K$  are negative, hence  $\Delta < 0$  and  $|\Delta| < 1$ . This means that the  $\tilde{H}_{XXZ}$  term represents an easy-plane XXZ model, whose low energy physics is described by the Luttinger liquid Hamiltonian. We will take  $\tilde{H}_{XXZ}$  as the unperturbed system and treat  $H_K$  and  $H_\Gamma$  as perturbations. Similar to Sec. IIIB,  $\tilde{H}_{XXZ}$  has a diverging Luttinger parameter when  $K \rightarrow 0$ . Therefore, the system is fragile to perturbations of the form  $e^{im\sqrt{\pi}\cos(\theta)}$  ( $m \in \mathbb{Z}$ ).

The symmetries in the original frame are given in Eq. (11), which become the following operations after the  $V_2$  transformation

$$\begin{aligned} V_2 T (V_2)^{-1} &= T, \\ V_2 T_a I (V_2)^{-1} &= R(\hat{z}, \pi) T_a I, \\ V_2 R(\hat{n}_1, \pi) T_a (V_2)^{-1} &= R(\hat{y}, \pi) R(\hat{z}, \frac{\pi}{2}) T_a. \end{aligned} \quad (72)$$

Under the symmetry operations in Eq. (72), the vertex operators  $e^{im\sqrt{\pi}\cos(\theta)}$  transform as

$$\begin{aligned} T &: \cos(m\sqrt{\pi}\theta) \rightarrow (-)^m \cos(m\sqrt{\pi}\theta), \\ &\quad \sin(m\sqrt{\pi}\theta) \rightarrow (-)^m \sin(m\sqrt{\pi}\theta), \\ R(\hat{z}, \pi) T_a I &: \cos(m\sqrt{\pi}\theta(x)) \rightarrow \cos(m\sqrt{\pi}\theta(-x)), \\ &\quad \sin(m\sqrt{\pi}\theta(x)) \rightarrow \sin(m\sqrt{\pi}\theta(-x)), \\ R(\hat{y}, \pi) R(\hat{z}, \frac{\pi}{2}) T_a &: \cos(m\sqrt{\pi}\theta) \rightarrow \cos(m\sqrt{\pi}\theta + \frac{m\pi}{2}), \\ &\quad \sin(m\sqrt{\pi}\theta) \rightarrow -\sin(m\sqrt{\pi}\theta - \frac{m\pi}{2}). \end{aligned} \quad (73)$$

As can be seen from Eq. (73), apart from the  $\cos(4\sqrt{\pi}\theta)$  term, the  $\sin(2\sqrt{\pi}\theta)$  term is also allowed by symmetries, which has a smaller scaling dimension than  $\cos(4\sqrt{\pi}\theta)$ . Keeping only the most relevant term, the low energy field theory becomes

$$\mathcal{H} = H_{LL} + u \int dx \sin(2\sqrt{\pi}\theta), \quad (74)$$

in which  $H_{LL}$  is the Luttinger liquid Hamiltonian describing the low energy physics of  $\tilde{H}_{XXZ}$ . To determine the magnetic pattern, we need to distinguish between the two cases  $u > 0$  and  $u < 0$ .

First consider the  $u > 0$  case. Then the  $u$  term in Eq. (74) is minimized at

$$\theta_n^{(I)} = (n - \frac{1}{4})\sqrt{\pi}, \quad 0 \leq n \leq 1, \quad (75)$$

which are two-fold degenerate. Take  $n = 0$  as an example. The spin ordering can be determined from the bosonization formulas in Eq. (30) as

$$\vec{S}_j^{(I)} = (-)^j \frac{1}{\sqrt{2}}(1, -1, 0)^T. \quad (76)$$

Performing  $(V_2)^{-1}$ , the magnetic pattern in the original frame is

$$\vec{S}_j^{(I)} = \frac{1}{\sqrt{2}}(1, -1, 0)^T. \quad (77)$$

The unbroken symmetry group can be determined as

$$H^{(I)} = \langle T_a I, R(\hat{n}_1, \pi) T_a \rangle, \quad (78)$$

and the most general form of the magnetic pattern invariant under  $H^{(I)}$  can be determined as

$$\vec{S}_j^{(I)} = N_3(1, -1, 0)^T, \quad (79)$$

where  $N_3$  is the magnitude of the spin ordering. Clearly, Eq. (79) is an FM order along  $\frac{1}{2}(1, -1, 0)^T$ -direction.

Next consider the  $u < 0$  case. Then the  $u$  term in Eq. (74) is minimized at

$$\theta_n^{(II)} = (n + \frac{1}{4})\sqrt{\pi}, \quad 0 \leq n \leq 1, \quad (80)$$

which are again two-fold degenerate. Take  $n = 0$  as an example. The spin ordering can be determined from the bosonization formulas in Eq. (30) as

$$\vec{S}_j^{(II)} = (-)^j \frac{1}{\sqrt{2}}(1, 1, 0)^T. \quad (81)$$

Performing  $(V_2)^{-1}$ , the magnetic pattern in the original frame is

$$\vec{S}_j^{(II)} = \frac{1}{\sqrt{2}}(1, 1, 0)^T. \quad (82)$$

The unbroken symmetry group can be determined as

$$H^{(II)} = \langle T_a I, TR(\hat{n}_1, \pi) T_a \rangle. \quad (83)$$

Notice that the magnetic ordering in Eq. (82) only represents a special configuration consistent with the unbroken symmetry group  $H^{(II)}$ . In fact, the most general form of the magnetic pattern invariant under  $H^{(II)}$  can be determined as

$$\vec{S}_j^{(II)} = (a, a, b)^T, \quad (84)$$

which is an FM order along  $\frac{1}{\sqrt{2a^2+b^2}}(a, a, b)^T$ -direction.

We note that the FM phase has been studied in Ref. 20, where DMRG numerics give the FM pattern in Eq. (84), indicating a negative  $u$ . The analysis in this section provides yet another explanation to the FM phase in the  $J < 0$  phase, complementing the several explanations for the origin of the FM phase in Ref. 20.

## VI. DMRG NUMERICS

In this section, we provide DMRG numerical evidences for the predictions in the previous sections.

We start with the Kitaev-Heisenberg model discussed in Sec. III. Fig. 5 shows the values of the central charge in the region  $\phi \in (\arctan(2), \pi/2)$  (where  $J = \cos(\phi)$ ,  $K = -\sin(\phi)$ ) extracted from entanglement entropy<sup>39</sup> at different system sizes with open boundary conditions. It can be observed from Fig. 5 that when  $\phi < 0.4\pi$ , the central charge value decreases by increasing system size, having a tendency to approach zero in the limit of infinite sizes. This is consistent with the analytic prediction in Sec. III on the existence of a magnetically ordered phase when  $\phi$  is close to  $\arctan(2)$ . On the other hand, when  $\phi > 0.4\pi$ , the value of the numerically extracted central charge increases by increasing the system size, tending to approach the value of 1 in the large size limit, thereby indicating a  $c = 1$  gapless phase in the region  $\phi \in (\arctan(2), \pi/2)$ . The low energy field theory describing this gapless phase is non-perturbative in nature, which remains unclear and will be left for future studies.

Notice that there are two possible types of magnetic orders according to the analysis in Sec. III and Sec. IV, namely, the spiral order and the LLRR order, both in the unrotated frame. In order to determine which type of magnetic order develops in the system, we study the response of the spin expectation values to a small uniform external magnetic field. When there is spontaneous symmetry breaking, it is known that an infinitesimal field is enough to produce finite spin expectation values in the thermodynamic limit.

For convenience, we perform DMRG numerics in the four-sublattice rotated frame, and accordingly, the patterns of spin expectation values of the spiral phase and the LLRR phase in the  $U_4$  frame are given by Eq. (61) and Eq. (65), respectively. When a uniform  $(1, 1, 0)$ -field is applied in the  $U_4$  frame, it is expected that the

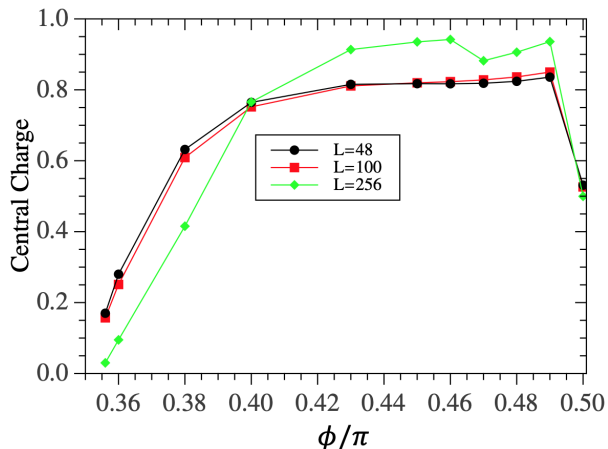


FIG. 4: Central charge values of the spin-1/2 Kitaev-Heisenberg chain as a function of  $\phi$ . DMRG numerics are performed for  $L = 48, 100, 256$  sites using open boundary conditions.

spin pattern in Eq. (61) is developed. Fig. 5 displays the numerical results of the spin expectation values at  $(\theta = 0.38\pi, \phi = 0.98\pi)$  when a  $h = 2 \times 10^{-4}$  field is applied along the  $(1, 1, 0)$ -direction. As can be seen from Fig. 5, the pattern is consistent with Eq. (61). On the other hand, when a uniform  $(0, 1, 0)$ -field is applied in the  $U_4$  frame, it is expected that the pattern in Eq. (65) develops in the system. Fig. 6 displays the numerical results of the spin expectation values at  $(\theta = 0.38\pi, \phi = 0.98\pi)$  when a  $h = 2 \times 10^{-4}$  field is applied along the  $(0, 1, 0)$ -direction. It can be observed from Fig. 6 that the pattern is consistent with Eq. (65).

To determine which type of magnetic orders wins, we study the change  $\Delta E$  in the ground state energy when magnetic fields in different directions are applied to the system. Fig. 7 shows the numerical results of the energy response to applied fields in the  $(1, 1, 0)$ - (blue) and  $(0, 1, 0)$ - (red) directions at  $(\theta = 0.38\pi, \phi = 0.98\pi)$ . As can be seen from Fig. 7, the system has a larger response to the  $(0, 1, 0)$ -field. Hence, it is the LLRR order that is developed in the system in the unrotated frame, rather than the spiral order.

## VII. WEAKLY COUPLED CHAINS: 2D STRIPY ORDER

Finally, we discuss how to obtain the 2D stripy order in the spin-1/2 Kitaev-Heisenberg model on the honeycomb lattice using a coupled-chain method based on the Luttinger liquid analysis. The generalization to the 2D spin-1/2 Kitaev-Heisenberg-Gamma model with a small nonzero Gamma interaction is straightforward.

The four-sublattice rotation in the 2D case is shown in Fig. 8, in which the sites marked with green, blue, yellow, and red colors are applied by  $R(\hat{y}, \pi)$ ,  $R(\hat{z}, \pi)$ ,

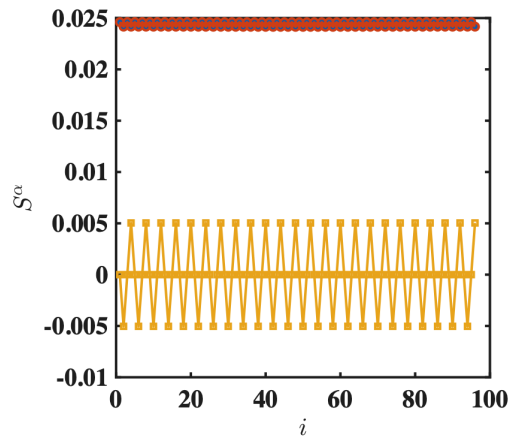


FIG. 5: Spin expectation values  $\langle S^x \rangle$  (marked with blue star),  $\langle S^y \rangle$  (marked with red circle), and  $\langle S^z \rangle$  (marked with yellow square) as functions of site  $i$  when a magnetic field  $h = 2 \times 10^{-4}$  is applied along the  $(1, 1, 0)$ -direction. DMRG numerics are carried out on a system of  $L = 96$  sites using periodic boundary conditions at  $(\theta = 0.38\pi, \phi = 0.98\pi)$  with a truncation error  $\epsilon = 10^{-10}$ .

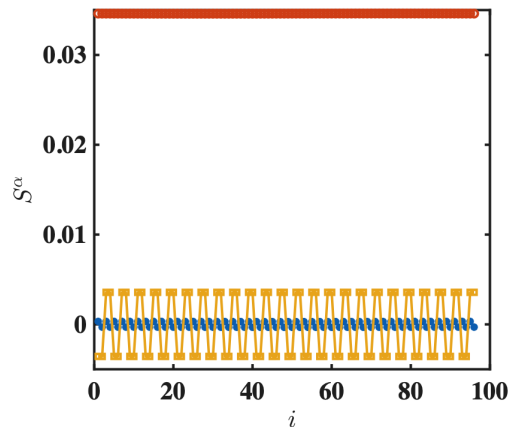


FIG. 6: Spin expectation values  $\langle S^x \rangle$  (marked with blue star),  $\langle S^y \rangle$  (marked with red circle), and  $\langle S^z \rangle$  (marked with yellow square) as functions of site  $i$  when a magnetic field  $h = 2 \times 10^{-4}$  is applied along the  $y$ -direction. DMRG numerics are carried out on a system of  $L = 96$  sites using periodic boundary conditions at  $(\theta = 0.38\pi, \phi = 0.98\pi)$  with a truncation error  $\epsilon = 10^{-10}$ . The data for  $\langle S^x \rangle$  and  $\langle S^y \rangle$  overlap and cannot be distinguished.

$R(\hat{x}, \pi)$ , and identity operations, respectively. After applying the four-sublattice rotation on the honeycomb lattice, the Hamiltonian of the Kitaev-Heisenberg model on bond  $\gamma$  in Fig. 8 acquires the form

$$H'_{ij} = (K_\gamma + 2J_\gamma)S'_i{}^\gamma S'_j{}^\gamma - J_\gamma \vec{S}'_i \cdot \vec{S}'_j, \quad (85)$$

in which  $K_x = K_y = K$ ,  $J_x = J_y = J$ ,  $\Gamma_x = \Gamma_y = \Gamma$ ,

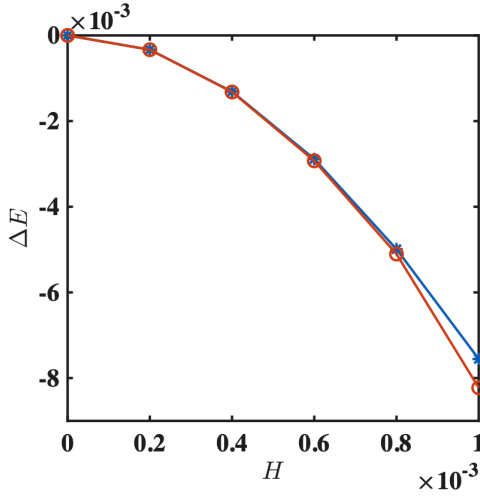


FIG. 7: Energy change  $\Delta E$  as a function of magnetic field along  $(1, 1, 0)$ - (blue) and  $(0, 1, 0)$ - (red) directions. DMRG numerics are performed on systems of  $L = 144$  sites using periodic boundary conditions at  $(\theta = 0.38\pi, \phi = 0.98\pi)$ .

$K_z = \alpha_0 K$ ,  $J_z = \alpha_0 J$ ,  $\Gamma_z = \alpha_0 \Gamma$ . We will consider the limit  $\alpha_0 \ll 1$ , i.e., the chains are weakly coupled.

Let's consider row  $c$  in in Fig. 8. When  $\alpha_0 = 0$ , the low energy theory of row  $c$  is described by the Luttinger liquid Hamiltonian

$$H_{cc} = \frac{v}{2} \int dx [\kappa^{-1} (\nabla \varphi)^2 + \kappa (\nabla \theta)^2] + g \int dx \cos(4\sqrt{\pi}\theta), \quad (86)$$

in which  $g < 0$  as discussed in Sec. III C. By performing a mean field treatment, the Hamiltonian of row  $c$  becomes

$$H'_c = H'_{cc} + H'_{cb} + H'_{cd}, \quad (87)$$

in which the interaction Hamiltonians  $H_{cb}$  and  $H_{cd}$  between row  $c$  and rows  $b, d$  are given by

$$H'_{cb} = \alpha_0 \sum_n [(K + 2J) S'_{c,2+2n} S'_{b,2+2n} - J \vec{S}'_{c,2+2n} \cdot \vec{S}'_{b,2+2n}] \quad (88)$$

and

$$H'_{cd} = \alpha_0 \sum_n [(K + 2J) S'_{c,1+2n} S'_{d,1+2n} - J \vec{S}'_{c,1+2n} \cdot \vec{S}'_{d,1+2n}]. \quad (89)$$

Performing  $(V_2)^{-1}$  to Eq. (30), we obtain

$$S'_c = C \sin(\sqrt{\pi}\theta), \quad (90)$$

in which  $C = \text{const.} \frac{1}{\sqrt{a}}$ . We consider the following ansatz

$$\vec{S}'_{c,j} = \vec{S}'_{b,j} = \vec{S}'_{d,j} = C \langle \sin(\sqrt{\pi}\theta) \rangle (0, 1, 0)^T. \quad (91)$$

Plugging Eq. (91) into Eq. (87), the mean field Hamiltonian can be simplified as

$$H'_c = \frac{v}{2} \int dx [\kappa^{-1} (\nabla \varphi)^2 + \kappa (\nabla \theta)^2] + g \int dx \cos(4\sqrt{\pi}\theta) - \alpha_0 C^2 \langle \sin(\sqrt{\pi}\theta) \rangle \int dx \sin(\sqrt{\pi}\theta). \quad (92)$$

Notice that  $\theta = \frac{1}{2}\sqrt{\pi}$  (corresponding to  $n = 1$  in Eq. (49)) can minimize both the  $g$  and  $\alpha_0$  terms in Eq. (92). Hence, in the  $U_4$  frame, the system has an FM order

$$\langle \vec{S}'_{i,j} \rangle \equiv A(0, 1, 0)^T, \quad (93)$$

in which  $A = C \langle \sin(\sqrt{\pi}\theta) \rangle$ .

Applying  $(U_4)^{-1}$  and rotating back to the original frame, the pattern of spin expectation values is shown in Fig. 8 (b), which is consistent with the results of classical analysis and exact diagonalization in Ref. 5. Notice that the pattern in Fig. 8 (b) is a 2D stripy order. Hence, we have obtained an explanation of the 2D stripy phase based on a quasi-1D Luttinger liquid analysis.

## VIII. SUMMARY

In summary, we have studied the phase diagram of the spin-1/2 Kitaev-Heisenberg chain in the  $(K < 0, J > 0)$  region, based on a combination of perturbative Luttinger liquid analysis and DMRG numerics. Close to the hidden  $SU(2)$  symmetric FM point, an ordered phase is identified having a left-left-right-right magnetic order, whereas close to the FM Kitaev point, a gapless phase with central charge value  $c = 1$  is found. The Luttinger liquid analysis is extended to the Kitaev-Heisenberg-Gamma model as well as the  $(K < 0, J < 0)$  region. Furthermore, the 2D stripy phase is recovered based on the 1D left-left-right-right order using a coupled-chain method, thereby providing a quasi-1D explanation for the stripy order on the honeycomb lattice.

## Acknowledgments

W.Y. is supported by the startup funding of Nankai University. C.X. acknowledges the supports from MOST grant No. 2022YFA1403900, NSFC No. 12104451, NSFC No. 11920101005, and funds from Strategic Priority Research Program of CAS No. XDB28000000. A.N. acknowledges computational resources and services provided by Compute Canada and Advanced Research Computing at the University of British Columbia. A.N. acknowledges support from the Max Planck-UBC-UTokyo Center for Quantum Materials and the Canada First Research Excellence Fund (CFREF) Quantum Materials and Future Technologies Program of the Stewart Blusson Quantum Matter Institute (SBQMI).

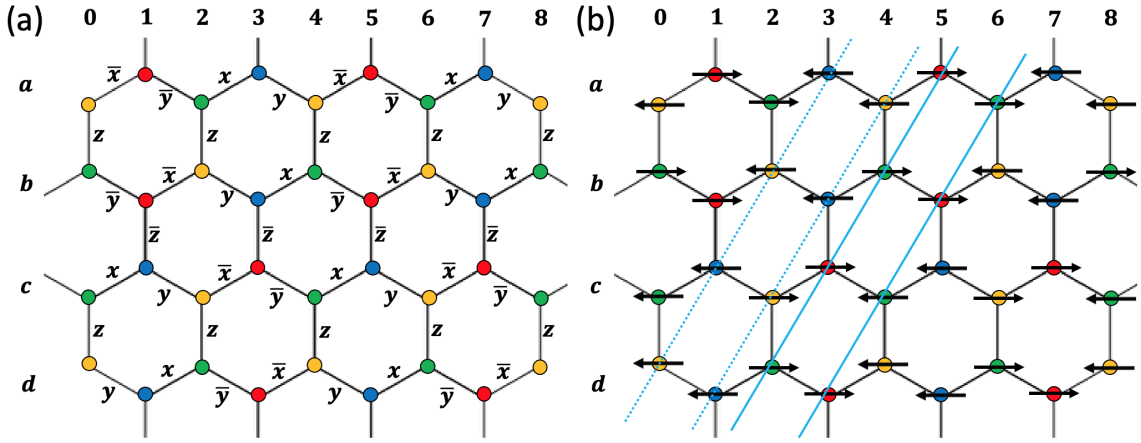


FIG. 8: (a) Four-sublattice rotation on the honeycomb lattice, and (b) stripy order in the original frame. In (b), the arrows represent the spin expectation values in the original frame which are along  $\pm\hat{y}$ -directions; the solid and dashed lines connect the sites which have the same spin expectation values.

### Appendix A: Symmetry transformation properties of the bosonization fields

In this appendix, we derive the transformation properties of the bosonization fields  $\theta, \varphi$  in Eq. (29) under symmetry transformations. Recall how the Luttinger liquid Hamiltonian  $H_{LL}$  is obtained. First, the spin operators are converted into spinless fermion operators under Jordan-Wigner transformation. Then the spinless fermion is rewritten in terms of the bosonic fields  $\theta, \varphi$  using the standard bosonization formalism. A noninteracting fermion model is obtained for the spin-1/2 XX chain, having  $\kappa = 1$  in Eq. (29). When the  $S^z S^z$  interaction is introduced, the Luttinger parameter  $\kappa$  will deviate from 1. Therefore, the strategy of obtaining the transformation properties of  $\theta, \varphi$  is to first derive the transformations of the spinless fermion fields using the known transformation properties of the spin operators, and then obtain how  $\theta, \varphi$  transform in the framework of bosonizing spinless fermions.

The Jordan-Wigner transformation defines the spinless fermion in terms of the spin operators, given by

$$c_j^\dagger = S_j^+ \prod_{k < j} (-2S_k^z), \quad (\text{A1})$$

which leads to

$$\begin{aligned} c_j &= S_j^- \prod_{k < j} (-2S_k^z), \\ c_j^\dagger c_j &= S_j^z + \frac{1}{2}. \end{aligned} \quad (\text{A2})$$

Using the following transformation properties of the spin operators,

$$\begin{aligned} T_a &: S_j^+ \rightarrow S_{j+1}^+, S_j^z \rightarrow S_j^z, \\ I &: S_j^+ \rightarrow S_{-j}^+, S_j^z \rightarrow S_{-j}^z, \\ T &: S_j^+ \rightarrow -S_j^-, S_j^z \rightarrow -S_j^z, \\ R(\hat{z}, \beta) &: S_j^+ \rightarrow e^{i\beta} S_j^+, S_j^z \rightarrow S_j^z, \\ R(\hat{y}, \pi) &: S_j^+ \rightarrow -S_j^-, S_j^z \rightarrow -S_j^z, \end{aligned} \quad (\text{A3})$$

the transformations of the spinless fermion can be obtained as

$$\begin{aligned} T_a &: c_j^\dagger \rightarrow c_{j+1}^\dagger, \\ I &: c_j^\dagger \rightarrow c_{-j}^\dagger \cdot \prod_{k \neq -j} (1 - 2c_k^\dagger c_k) = c_{-j}^\dagger e^{i\pi S_T^z}, \\ T &: c_j^\dagger \rightarrow (-)^\# (-)^j c_j, \\ R(\hat{z}, \beta) &: c_j^\dagger \rightarrow e^{i\beta} c_j^\dagger, \\ R(\hat{y}, \pi) &: c_j^\dagger \rightarrow (-)^\# (-)^j c_j, \end{aligned} \quad (\text{A4})$$

in which  $S_T^z (\in \mathbb{Z})$  is the total spin of the system. In the transformation rules under  $T$  and  $R(\hat{y}, \pi)$ , the staggered sign  $(-)^j$  comes from the factor of the string  $\prod_{k < j} (2S_k^z)$ . There is an indefinite sign  $(-)^{\#}$  since the overall sign should be  $\prod_{k \leq j} (-)$ , which is not well-defined for a chain of infinite length (we need to consider an infinite chain so that linearization around Fermi points and low energy fields can be considered).

For a spin-1/2 XX chain, the system is converted into a non-interacting spinless fermion after the Jordan-Wigner transformation. The low energies physics is dominated by the two gapless points  $\pm k_F$ , in which  $k_F = \pi/(2a)$  where  $a$  is the lattice constant. Introducing the left and right movers  $c_L^\dagger, c_R^\dagger$ , the bosonized fields  $\theta, \varphi$  can be related to the fermion fields as

$$\begin{aligned}\varphi(x) &= \varphi_0 - (N_L + N_R)\sqrt{\pi}x/L - i \sum_{q \neq 0} \left| \frac{1}{2qL} \right|^{1/2} \text{sgn}(q) e^{iqx} (b_q^\dagger + b_{-q}), \\ \theta(x) &= \theta_0 + (N_L - N_R)\sqrt{\pi}x/L + i \sum_{q \neq 0} \left| \frac{1}{2qL} \right|^{1/2} e^{iqx} (b_q^\dagger - b_{-q}),\end{aligned}\tag{A5}$$

in which  $L$  is the system size;  $N_r$  ( $r = L, R$ ) is the (normal ordered) total fermion number in the  $r$ -branch satisfying  $S_T^z = N_L + N_R$ ; and

$$b_q^\dagger = \left| \frac{2\pi}{qL} \right|^{1/2} [\Theta(q)\rho_R^\dagger(q) + \Theta(-q)\rho_L^\dagger(q)],\tag{A6}$$

where  $\Theta$  is the step function and

$$\rho_r(q) = \sum_k c_{r, k+q}^\dagger c_{r, k}, \quad r = L, R.\tag{A7}$$

In Eq. (A5), the constant fields  $\varphi_0$  and  $\theta_0$  are the canonical conjugate fields of  $N_L - N_R$  and  $N_L + N_R$ , respectively, satisfying

$$[N_L - N_R, \varphi_0] = [N_L + N_R, \theta_0] = \frac{i}{\sqrt{\pi}}.\tag{A8}$$

In fact,  $\varphi_0$  represents the center of mass position of all the fermion, and  $\theta_0$  represents the center of mass phase of the fermions.

The translation operators are generated by the total momentum, i.e.,  $k_F(N_L - N_R)$ . It is clear that the translation operator does not change the components in  $\theta(x), \varphi(x)$  except  $\theta_0, \varphi_0$ . Hence  $T_a = e^{ik_F a(N_L - N_R)} = e^{i(N_L - N_R)\pi/2}$ . Using Eq. (A8), we obtain

$$T_a \varphi_0 T_{-a} = \varphi_0 + \frac{\sqrt{\pi}}{2}.\tag{A9}$$

To derive how  $T_a$  acts on  $\theta_0$ , we need the following bosonization formula for  $c^\dagger(x)$ ,

$$c^\dagger(x) = \eta_R^\dagger e^{ik_F x} e^{i\sqrt{\pi}[\theta(x) - \varphi(x)]} + \eta_L^\dagger e^{-ik_F x} e^{i\sqrt{\pi}[\theta(x) + \varphi(x)]},\tag{A10}$$

in which  $\eta_R$  and  $\eta_L$  are the Klein factors for the right and left movers. Since  $e^{\pm ik_F x}$  differs from  $e^{\pm ik_F(x+a)}$  by a factor of  $\pm i$ , we must have

$$\begin{aligned}T_a e^{i\sqrt{\pi}[\theta(x) - \varphi(x)]} T_{-a} &= i e^{i\sqrt{\pi}[\theta(x) - \varphi(x)]}, \\ T_a e^{i\sqrt{\pi}[\theta(x) + \varphi(x)]} T_{-a} &= -i e^{i\sqrt{\pi}[\theta(x) + \varphi(x)]}.\end{aligned}\tag{A11}$$

On the other hand, Eq. (A9) implies  $T_a e^{i\sqrt{\pi}\varphi(x)} T_{-a} = i e^{i\sqrt{\pi}\varphi(x)}$ , hence  $T_a e^{i\sqrt{\pi}\theta(x)} T_{-a} = -e^{i\sqrt{\pi}\theta(x)}$ , i.e.,

$$T_a \theta_0 T_{-a} = \theta_0 + \sqrt{\pi}.\tag{A12}$$

Thus we obtain

$$\begin{aligned}T_a \theta(x) T_{-a} &= \theta(x) + \sqrt{\pi}, \\ T_a \varphi(x) T_{-a} &= \varphi(x) + \frac{\sqrt{\pi}}{2}, \\ T_a \eta_r^\dagger T_{-a} &= \eta_r^\dagger,\end{aligned}\tag{A13}$$

in which  $r = L, R$ .

Define  $\theta'(x)$  ( $\varphi'(x)$ ) to be the components of  $\theta(x)$  ( $\varphi(x)$ ) excluding  $\theta_0$  ( $\varphi_0$ ). Since

$$\begin{aligned} I\rho_r(q)I^{-1} &= \rho_{-r}(-q) \\ IN_rI^{-1} &= N_{-r} \end{aligned} \quad (\text{A14})$$

where  $-L = R$  and  $-R = L$ . For the inversion operation, it can be seen that

$$\begin{aligned} I\theta'(x)I^{-1} &= \theta'(-x) \\ I\varphi'(x)I^{-1} &= -\varphi'(-x). \end{aligned} \quad (\text{A15})$$

To derive the transformations of  $\theta_0, \varphi_0$ , we use Eq. (A10) to rewrite the second equation in Eq. (A4) and obtain

$$\begin{aligned} &e^{ik_Fx}I\eta_R^\dagger e^{i\sqrt{\pi}[\theta(x)-\varphi(x)]}I^{-1} + e^{-ik_Fx}I\eta_L^\dagger e^{i\sqrt{\pi}[\theta(x)+\varphi(x)]}I^{-1} \\ &= (\eta_R^\dagger e^{-ik_Fx} e^{i\sqrt{\pi}[\theta(-x)-\varphi(-x)]} + \eta_L^\dagger e^{ik_Fx} e^{i\sqrt{\pi}[\theta(-x)+\varphi(-x)]})e^{i\pi(N_L+N_R)}, \end{aligned} \quad (\text{A16})$$

which leads to

$$\begin{aligned} I\theta_0I^{-1} &= \theta_0, \\ I\varphi_0I^{-1} &= -\varphi_0 + \sqrt{\pi}(N_L + N_R), \\ I\eta_L^\dagger I^{-1} &= \eta_R^\dagger, \\ I\eta_R^\dagger I^{-1} &= \eta_L^\dagger. \end{aligned} \quad (\text{A17})$$

Notice that in Eq. (A17), the fact that whether  $e^{i\pi(N_L+N_R)}$  or  $e^{-i\pi(N_L+N_R)}$  is used in Eq. (A21) does not matter. Combining Eq. (A15) with Eq. (A17), we obtain

$$\begin{aligned} I\theta(x)I^{-1} &= \theta(x), \\ I\varphi(x)I^{-1} &= -\varphi(x) + \sqrt{\pi}(N_L + N_R), \\ I\eta_r^\dagger I^{-1} &= \eta_{-r}^\dagger. \end{aligned} \quad (\text{A18})$$

For time reversal, using

$$\begin{aligned} T\rho_r(q)T^{-1} &= -\rho_{-r}(-q), \\ TN_rT^{-1} &= -N_{-r}, \end{aligned} \quad (\text{A19})$$

we have

$$\begin{aligned} T\theta'(x)T^{-1} &= \theta'(x) \\ T\varphi'(x)T^{-1} &= -\varphi'(x). \end{aligned} \quad (\text{A20})$$

To derive the transformations of  $\theta_0, \varphi_0$ , we use Eq. (A10) to rewrite the third equation in Eq. (A4) and obtain

$$\begin{aligned} &e^{-ik_Fx}T\eta_R^\dagger e^{i\sqrt{\pi}[\theta(x)-\varphi(x)]}T^{-1} + e^{ik_Fx}T\eta_L^\dagger e^{i\sqrt{\pi}[\theta(x)+\varphi(x)]}T^{-1} \\ &= (-)^\# [\eta_R e^{ik_Fx} e^{-i\sqrt{\pi}[\theta(x)-\varphi(x)]} + \eta_L e^{-ik_Fx} e^{-i\sqrt{\pi}[\theta(x)+\varphi(x)]}], \end{aligned} \quad (\text{A21})$$

leading to

$$\begin{aligned} T\theta_0T^{-1} &= \theta_0 + \#\sqrt{\pi}, \\ T\varphi_0T^{-1} &= -\varphi_0, \\ T\eta_R^\dagger T^{-1} &= \eta_L, \\ T\eta_L^\dagger T^{-1} &= \eta_R. \end{aligned} \quad (\text{A22})$$

The indefinite coefficient  $\#$  can be determined to be 1 by imposing the condition  $T\vec{S}_i T^{-1} = -\vec{S}_i$  from the bosonization formulas for the spin operators in Eq. (30). Combining Eq. (A20) with Eq. (A22), we have

$$\begin{aligned} T\theta(x)T^{-1} &= \theta(x) + \sqrt{\pi}, \\ T\varphi(x)T^{-1} &= -\varphi(x), \\ T\eta_r^\dagger T^{-1} &= \eta_{-r}. \end{aligned} \quad (\text{A23})$$

The generator for the U(1) transformation  $R(\hat{z}, \beta)$  is  $N_L + N_R$ . Using the commutation relation in Eq. (A8), it is straightforward to derive that

$$\begin{aligned} R(\hat{z}, \beta)\theta(x)[R(\hat{z}, \beta)]^{-1} &= \theta(x) + \frac{\beta}{\sqrt{\pi}}, \\ R(\hat{z}, \beta)\varphi(x)[R(\hat{z}, \beta)]^{-1} &= \varphi(x), \\ R(\hat{z}, \beta)\eta_r^\dagger[R(\hat{z}, \beta)]^{-1} &= \eta_r^\dagger. \end{aligned} \quad (\text{A24})$$

For  $R(\hat{y}, \pi)$ , using

$$\begin{aligned} R(\hat{y}, \pi)\rho_r(q)[R(\hat{y}, \pi)]^{-1} &= -\rho_r(q), \\ R(\hat{y}, \pi)N_r[R(\hat{y}, \pi)]^{-1} &= -N_r(q), \end{aligned} \quad (\text{A25})$$

we obtain

$$\begin{aligned} R(\hat{y}, \pi)\theta'(x)[R(\hat{y}, \pi)]^{-1} &= -\theta'(x) \\ R(\hat{y}, \pi)\varphi'(x)[R(\hat{y}, \pi)]^{-1} &= -\varphi'(x). \end{aligned} \quad (\text{A26})$$

To derive the transformations of  $\theta_0, \varphi_0$ , we use Eq. (A10) to rewrite the fifth equation in Eq. (A4) and obtain

$$\begin{aligned} e^{ik_F x} R(\hat{y}, \pi)\eta_R^\dagger e^{i\sqrt{\pi}[\theta(x)-\varphi(x)]}[R(\hat{y}, \pi)]^{-1} + e^{-ik_F x} R(\hat{y}, \pi)\eta_L^\dagger e^{i\sqrt{\pi}[\theta(x)+\varphi(x)]}[R(\hat{y}, \pi)]^{-1} = \\ (-)\# [\eta_R e^{ik_F x} e^{-i\sqrt{\pi}[\theta(x)-\varphi(x)]} + \eta_L e^{-ik_F x} e^{-i\sqrt{\pi}[\theta(x)+\varphi(x)]}], \end{aligned} \quad (\text{A27})$$

leading to

$$\begin{aligned} R(\hat{y}, \pi)\theta_0[R(\hat{y}, \pi)]^{-1} &= -\theta_0 + \#\sqrt{\pi}, \\ R(\hat{y}, \pi)\varphi_0[R(\hat{y}, \pi)]^{-1} &= -\varphi_0, \\ R(\hat{y}, \pi)\eta_R^\dagger[R(\hat{y}, \pi)]^{-1} &= \eta_R, \\ R(\hat{y}, \pi)\eta_L^\dagger[R(\hat{y}, \pi)]^{-1} &= \eta_L, \end{aligned} \quad (\text{A28})$$

where the indefinite sign can be determined in a similar way as the time reversal case to be  $\sqrt{\pi}$ . Combining Eq. (A26) with Eq. (A28), we have

$$\begin{aligned} R(\hat{y}, \pi)\theta(x)[R(\hat{y}, \pi)]^{-1} &= -\theta(x) + \sqrt{\pi}, \\ R(\hat{y}, \pi)\varphi(x)[R(\hat{y}, \pi)]^{-1} &= -\varphi(x), \\ R(\hat{y}, \pi)\eta_r^\dagger[R(\hat{y}, \pi)]^{-1} &= \eta_r. \end{aligned} \quad (\text{A29})$$

In summary, we are able to derive the transformation properties in Eq. (32). We note that the transformation rules of  $\vec{S}_i$  in Eq. (A3) can be obtained, by particularly noticing that rigorously, the expression of  $S_j^z$  is

$$S^z(x) = -\frac{1}{\sqrt{\pi}}\nabla\varphi(x) + \text{const.} \frac{1}{a}(-)^n [\eta_R^\dagger \eta_L e^{i2\sqrt{\pi}\varphi(x)} + \eta_L^\dagger \eta_R e^{-i2\sqrt{\pi}\varphi(x)}]. \quad (\text{A30})$$

<sup>1</sup> A. Kitaev, *Anyons in an exactly solved model and beyond*, Ann. Phys. (N. Y). **321**, 2 (2006).

<sup>2</sup> C. Nayak, S. H. Simon, A. Stern, M. Freedman, and S. Das Sarma, *Non-Abelian anyons and topological quantum computation*, Rev. Mod. Phys. **80**, 1083 (2008).

<sup>3</sup> G. Jackeli and G. Khaliullin, *Mott insulators in the strong spin-orbit coupling limit: from Heisenberg to a quantum compass and Kitaev models*, Phys. Rev. Lett. **102**, 017205 (2009).

<sup>4</sup> J. Chaloupka, G. Jackeli, and G. Khaliullin, *Kitaev-Heisenberg Model on a Honeycomb Lattice: Possible Exotic Phases in Iridium Oxides  $A_2\text{IrO}_3$* , Phys. Rev. Lett. **105**, 027204 (2010).

<sup>5</sup> J. G. Rau, E. K. H. Lee, and H. Y. Kee, *Generic spin model for the honeycomb iridates beyond the Kitaev limit*, Phys. Rev. Lett. **112**, 077204 (2014).

<sup>6</sup> I. Kimchi and A. Vishwanath, *Kitaev-Heisenberg models for iridates on the triangular, hyperkagome, kagome, fcc*,

- and pyrochlore lattices, *Phys. Rev. B* **89**, 014414 (2014).
- 7 W. Wang, Z.-Y. Dong, S.-L. Yu, and J.-X. Li, *Theoretical investigation of magnetic dynamics in  $\alpha$ - $\text{RuCl}_3$* , *Phys. Rev. B* **96**, 115103 (2017).
  - 8 W. Witczak-Krempa, G. Chen, Y. B. Kim, and L. Balents, *Correlated quantum phenomena in the strong spin-orbit regime*, *Annu. Rev. Condens. Matter Phys.* **5**, 57 (2014).
  - 9 J. G. Rau, E. K.-H. Lee, and H.-Y. Kee, *Spin-orbit physics giving rise to novel phases in correlated systems: Iridates and related materials*, *Annu. Rev. Condens. Matter Phys.* **7**, 195 (2016).
  - 10 S. M. Winter, A. A. Tsirlin, M. Daghofer, J. van den Brink, Y. Singh, P. Gegenwart, and R. Valentí, *J. Phys. Condens. Matter* **29**, 493002 (2017).
  - 11 M. Hermanns, I. Kimchi, and J. Knolle, *Models and materials for generalized Kitaev magnetism*, *Annu. Rev. Condens. Matter Phys.* **9**, 17 (2018).
  - 12 E. Sela, H.-C. Jiang, M. H. Gerlach, and S. Trebst, *Order-by-disorder and spin-orbital liquids in a distorted Heisenberg-Kitaev model*, *Phys. Rev. B* **90**, 035113 (2014).
  - 13 J. H. Gruenewald, J. Kim, H. S. Kim, J. M. Johnson, J. Hwang, M. Souri, J. Terzic, S. H. Chang, A. Said, J. W. Brill, G. Cao, H.-Y. Kee, S. S. A. Seo, *Engineering 1D quantum stripes from superlattices of 2D layered materials* *Advanced Materials* **29**, 163798 (2017).
  - 14 C. E. Agrapidis, J. van den Brink, and S. Nishimoto, *Ordered states in the Kitaev-Heisenberg model: From 1D chains to 2D honeycomb*, *Sci. Rep.* **8**, 1815 (2018).
  - 15 C. E. Agrapidis, J. van den Brink, and S. Nishimoto, *Ground state and low-energy excitations of the Kitaev-Heisenberg two-leg ladder*, *Phys. Rev. B* **99**, 224418 (2019).
  - 16 A. Catuneanu, E. S. Sørensen, and H.-Y. Kee, *Nonlocal string order parameter in the  $S = \frac{1}{2}$  Kitaev-Heisenberg ladder*, *Phys. Rev. B* **99**, 195112 (2019).
  - 17 Z.-A. Liu, T.-C. Yi, J.-H. Sun, Y.-L. Dong, and W.-L. You, *Lifshitz phase transitions in a one-dimensional Gamma model*, *Phys. Rev. E* **102**, 032127 (2020).
  - 18 W.-L. You, G. Sun, J. Ren, W. C. Yu, and A. M. Oleś, *Quantum phase transitions in the spin-1 Kitaev-Heisenberg chain*, *Phys. Rev. B* **102**, 144437 (2020).
  - 19 W. Yang, A. Nocera, T. Tummuru, H.-Y. Kee, and I. Affleck, *Phase Diagram of the Spin-1/2 Kitaev-Gamma Chain and Emergent  $SU(2)$  Symmetry*, *Phys. Rev. Lett.* **124**, 147205 (2020).
  - 20 W. Yang, A. Nocera, and I. Affleck, *Comprehensive study of the phase diagram of the spin- $\frac{1}{2}$  Kitaev-Heisenberg-Gamma chain*, *Phys. Rev. Research* **2**, 033268 (2020).
  - 21 W. Yang, A. Nocera, and I. Affleck, *Spin wave theory of a one-dimensional generalized Kitaev model*, *Phys. Rev. B* **102**, 134419 (2020).
  - 22 W. Yang, A. Nocera, E. S. Sørensen, H.-Y. Kee, and I. Affleck, *Classical spin order near the antiferromagnetic Kitaev point in the spin- $\frac{1}{2}$  Kitaev-Gamma chain*, *Phys. Rev. B* **103**, 054437 (2021).
  - 23 Q. Luo, J. Zhao, X. Wang, and H.-Y. Kee, *Unveiling the phase diagram of a bond-alternating spin- $\frac{1}{2}$   $K$ - $\Gamma$  chain*, *Phys. Rev. B* **103**, 144423 (2021).
  - 24 Q. Luo, S. Hu, and H.-Y. Kee, *Unusual excitations and double-peak specific heat in a bond-alternating spin-1  $K$ - $\Gamma$  chain*, *Phys. Rev. Research* **3**, 033048 (2021).
  - 25 E. S. Sørensen, A. Catuneanu, J. Gordon, H.-Y. Kee, *Heart of entanglement: Chiral, nematic, and incommensurate phases in the Kitaev-Gamma ladder in a field*, *Phys. Rev. X* **11**, 011013 (2021).
  - 26 W. Yang, A. Nocera, P. Herrer, R. Raussendorf, I. Affleck, *Symmetry analysis of bond-alternating Kitaev spin chains and ladders*, *Phys. Rev. B* **105**, 094432 (2022).
  - 27 Wang Yang, Chao Xu, Shenglong Xu, Alberto Nocera, Ian Affleck, *Nonsymmorphic Luttinger liquids in generalized antiferromagnetic Kitaev spin-1/2 chain*, *Phys. Rev. B* **109**, L180403 (2024).
  - 28 W. Yang, C. Xu, A. Nocera, I. Affleck, *Origin of nonsymmorphic bosonization formulas in generalized antiferromagnetic Kitaev spin- $\frac{1}{2}$  chains from a renormalization-group perspective*, *Phys. Rev. B* **106**, 064425 (2022).
  - 29 W. Yang, A. Nocera, C. Xu, A. Adhikary, I. Affleck, *Emergent  $SU(2)_1$  conformal symmetry in the spin-1/2 Kitaev-Gamma chain with a Dzyaloshinskii-Moriya interaction*, arXiv:2204.13810 (2022).
  - 30 W. Yang, A. Nocera, C. Xu, I. Affleck, *Nonsymmorphic spin-space cubic groups and  $SU(2)_1$  conformal invariance in one-dimensional spin-1/2 models*, arXiv:2208.10754 (2022).
  - 31 W. Yang, A. Nocera, C. Xu, H.-Y. Kee, I. Affleck, *Counterrotating spiral, zigzag, and  $120^\circ$  orders from coupled-chain analysis of Kitaev-Gamma-Heisenberg model, and relations to honeycomb iridates*, arXiv:2207.02188 (2022).
  - 32 Z. Zhao, T.-C. Yi, M. Xue, and W.-L. You, *Characterizing quantum criticality and steered coherence in the XY-Gamma chain*, *Phys. Rev. A* **105**, 063306 (2022).
  - 33 P. Laurell, G. Alvarez, E. Dagotto, *Spin dynamics of the generalized quantum spin compass chain*, arXiv:2210.00357 (2022).
  - 34 J. Chaloupka, G. Jackeli, and G. Khaliullin, *Zigzag Magnetic Order in the Iridium Oxide  $\text{Na}_2\text{IrO}_3$* , *Phys. Rev. Lett.* **110**, 097204 (2013).
  - 35 J. Chaloupka, and G. Khaliullin, *Hidden symmetries of the extended Kitaev-Heisenberg model: Implications for the honeycomb-lattice iridates  $\text{A}_2\text{IrO}_3$* , *Phys. Rev. B* **92**, 024413 (2015).
  - 36 S. R. White, *Density matrix formulation for quantum renormalization groups*, *Phys. Rev. Lett.* **69**, 2863 (1992).
  - 37 S. R. White, *Density-matrix algorithms for quantum renormalization groups*, *Phys. Rev. B* **48**, 10345 (1993).
  - 38 U. Schollwöck, *The density-matrix renormalization group in the age of matrix product states*, *Ann. Phys. (N. Y.)* **326**, 96 (2011).
  - 39 P. Calabrese and J. Cardy, *J. Phys. A* **42**, 504005 (2009).
  - 40 One can actually consider  $G_0/\langle T_{2a} \rangle$  for the Kitaev-Heisenberg model, but  $T_{4a}$  is considered instead so that we can conveniently compare  $G_0/\langle T_{4a} \rangle$  with the symmetry group of the Kitaev-Heisenberg-Gamma model in the  $U_4$  frame later.